Auxiliary Information for

"Wind-blown sandstones cemented by sulfate and clay minerals in Gale Crater, Mars" R.E. Milliken, R.C. Ewing, W.W. Fischer, and J. Hurowitz

Distribution and Additional Examples of Fractures and Preserved Bedforms in Gale Crater

The lowermost strata in the Lower fm. of Mt. Sharp exhibit features consistent with eolian sandstones that may be cemented by sulfates. As described in the main text, parallel bounding surfaces and low-angle stratification in Lower Mt. Sharp are similar to features observed in terrestrial eolian sandstones such as the Navajo sandstone in the southwestern U.S. (Figure A1). These strata in Mt. Sharp (e.g., Figure A1b,c) may originate from eolian processes similar to what has been observed in Meridiani Planum by the Opportunity rover [*Grotzinger et al.*, 2005]. As with the Meridiani deposits, the Lower fm. of Mt. Sharp is also known to host sulfate salts, and these minerals may be the cementing agent in an otherwise basaltic sandstone. Although laterally equivalent and overlying strata exhibit spectral features indicative of sulfates [*Milliken et al., 2010*], additional orbital visible-near infrared reflectance spectra are needed to confirm if this exact location also hosts sulfate salts.

Figure A2 presents examples of filled fractures, possible diagenetic overprinting, and evidence of post-depositional fluid flow in the Lower formation in support of discussion provided in the main text. Numerous filled fractures throughout Gale Crater and Mt. Sharp indicate that these sandstones and other strata of the Lower fm. have experienced post-depositional fluid flow and likely mineralization in fractures and pore space (distribution and locations shown in Figure A2a). Such filled fractures have been observed in other locations on Mars [*Okubo and McEwen*, 2007], and in Gale they often occur as complex intersecting networks of raised ridges, consistent with mineral-induced strengthening. Their occurrence at various stratigraphic levels in the Lower fm., as well as in the 'mound skirting unit' with the 'washboard' texture that surrounds and in some cases clearly onlaps the Lower fm., suggests that post-depositional fluid circulation was widespread within Gale Crater and may have been an important diagenetic process over a significant period of time.

In addition, a section in the southwest portion of the Lower formation in Mt. Sharp is characterized by a lack of clear, continuous, parallel bedding, which is in contrast to the strata immediately above and below this zone that exhibit these characteristics (Figure A2g,h). This disordered and degraded region may represent a zone of recrystallization, where migrating fluids dissolved existing pore-filling cements, wiping out clear bedding contacts and producing the rough texture observed in HiRISE images. This zone is bounded on its upper and lower limits by remarkably well-defined beds, which are also characteristic of the northwestern portion of the Lower fm. that Curiosity will explore. Though admittedly speculative, this region may represent a zone of recrystallization, consistent with the detections of highly soluble Mg-sulfates in the Lower fm. and other features that indicate post-depositional fluid circulation.

As described in the main body of the text, there are numerous occurrences of what we interpret to be preserved bedforms and erosional remnants of such features (e.g., 'washboard' texture) on the crater floor units directly adjacent to Mt. Sharp as well as in Mt. Sharp itself (Figures 2-4). Additional examples of these features that we have observed in Gale are presented here in Figures A3-A5. Crestline bifurcations are one of the key evidences we use to interpret the widespread linear features as bedforms. Crestline bifurcations occur in bedforms generated in marine, fluvial and aeolian environments and in both unidirectional and oscillatory flow. Bifurcations are a hallmark of migrating bedforms where one crestline interacts with an adjacent bedform in the downflow direction. The, straight-crested, regularly and widely spaced (50+ meters) crestlines and the widespread presence of aeolian bedforms on Mars and in Mars' stratigraphic record provide the basis for the interpretation that these are aeolian bedforms. In the 'mound skirting unit' mapped by *Anderson and Bell* [2010], the morphology is often expressed as localized, roughly linear, flat-topped mesas that are surrounded by topographically lower light-toned strata. This 'washboard' morphology is consistent with the partial erosion of preserved bedforms, in which interdune sediments or upper bounding surfaces of the stoss sides of dunes are preserved and dune crests are preferentially eroded (Figure 2, A5). However, the relationships between wholly preserved bedforms (Figure A4) and the washboard morphology (Figure A5) are not always clear because they often do not appear in direct contact with one another. The two examples presented in this paper (Figures 2, A5) are the only locations we have observed where both morphologies are present and appear to grade into one another. It is clear that the relationships are complex, and though our preferred interpretation is that the 'washboard' morphology can result from preferential cementation/preservation of interdune sediments, the variability in morphologic expression of the 'washboard' unit leaves the door open for multiple formation mechanisms. Regardless, all mechanisms for formation of the 'washboard' morphology are consistent with the initial presence of bedforms, either wholly or partially lithified.

The wide spatial distribution of preserved bedforms and the variable degree of their state of preservation (Figure A3) suggests that eolian processes were common during the period in which the Lower fm. was formed and their degree of cementation/lithification is variable. Though some occurrences of preserved bedforms are associated with clay mineral signatures (Figure 4, A6-A8), most of the bedforms shown in Figure A3 exhibit no unique spectral signatures or lack CRISM coverage. In addition to clay minerals or sulfate salts, the bedforms may also be partially cemented by small abundances of silica, and if this silica is not hydrated (i.e., it is quartz), then it would be undetectable at the wavelengths of CRISM. Therefore, although the cementing agent is not known for all occurrences of preserved bedforms, their existence and the remarkable degree to which even the crests are wholly preserved requires that they be at least partially lithified. Preservation would also be enhanced by early and rapid burial, possibly by fine-grained sediments. This is consistent with the occurrence of preserved bedforms under fan deposits sourced from the Lower fm. (Figures A3, A4). In summary, the morphological and mineralogical data indicate that conditions of early cementation and rapid burial were key in the preservation of the bedforms, and these conditions could have been met by either rising groundwater that breached the surface or by relatively low-energy overland flow that flooded the dune fields without producing significant erosion of the original dune topography.

CRISM Data Processing Methods and Spectral Identification of Minerals

Visible-near infrared reflectance spectra (0.36 - 3.92 μm) acquired by the Compact Reconnaissance Imaging Spectrometer for Mars (CRISM) instrument used for this work were processed following standard techniques employed by the CRISM instrument team [*Murchie et al.*, 2009]. CRISM acquires spectral images of the Martian surface in two basic modes: global 'mapping' (multispectral survey) mode and high-resolution 'targeted' mode. In the lower resolution mapping mode, radiance is measured at 72 wavelengths and a spatial resolution of ~100-200 m/pixel, allowing rough detection of possibly hydrated minerals on relatively large scales. In the targeted mode, all 544 wavelength channels are used and the spatial resolution can vary from ~18 m/pixel (Full Resolution Target, FRT) to ~36 m/pixel (Half Resolution Target, HRL). For this work, CRISM data are converted to apparent I/F and although atmospheric gas absorptions are minimized there is no attempt to independently model the abundance of atmospheric aerosols. The instrument background was subtracted from raw data using measurements when an internal shutter was closed,and the result is scaled to radiance by dividing by comparably processed measurements of an internal integrating sphere and multiplying by a radiometric model of the sphere constructed during ground calibration. I/F is determined by dividing radiance by the solar irradiance scaled for the appropriate Sun-Mars distance. Photometric effects are modeled by dividing the result by the cosine of the incidence angle. A scaled atmospheric transmission spectrum is used to account for atmospheric effects (gases). This observation was obtained by CRISM over a crossing of the Olympus Mons volcano and can be used to derive an approximation to an atmospheric transmission spectrum.

Broad residual trends may remain if the aerosols' nature and abundance has shifted over time relative to the timing of this 'volcano scan', and this is often the case. However, our analysis is based on narrow vibrational absorption features (e.g., metal-OH absorptions), and while residual aerosols may affect whether or not surface spectral features are observed at all (increased opacity leads to decreased measurements in surface radiance), such aerosol effects will not affect our interpretation of surface spectral features that can be observed. Variabilities in atmospheric conditions are a common reason why overlapping CRISM images may yield different results in the detection of hydrated minerals at the surface, especially if the detections are relatively weak to begin with. Detection of weak spectral signatures is also complicated by significantly reduced instrument signal to noise ratio (SNR) values due to increased detector temperatures.

Although CRISM has acquired many observations over Gale Crater and Mt. Sharp, many of these observations are limited in use due to poor atmospheric conditions (high opacity that masks surface features) and/or detector temperatures that are warmer than nominal conditions. This necessitates averaging many pixels together to retrieve surface reflectance spectra in which absorption features of interest are clearly stronger than random channel-to-channel variations. Spectral features of interest, such as those associated with hydrated clay minerals or sulfate salts, can be further accentuated by dividing a spectrum by one from a nearby pixel that appears to lack the features of interest. This process of 'spectral ratios' has been commonly employed by the CRISM team in many previous publications [e.g., Murchie et al., 2009]. Here, we average spectra from a region of interest (ROI) and divide that average by the spectral average from another ROI. The latter is ideally taken over a region that appears to lack the spectral features of interest, often a dust or soil-covered region when attempting to isolate clay mineral or sulfate

spectral features. However, the typical footprint of a CRISM FRT image is ~10 x 10 km, and this footprint does not always include a dusty or otherwise spectrally 'bland' region. In these cases, the spectral average used in the denominator may include broad absorptions near ~1 and ~2 μm associated with Fe in minerals such as olivine or pyroxene, resulting in broad peaks at these wavelength positions in the resulting spectral ratios.

In all spectra presented here and in the main text, great care has been taken to ensure that the spectral features we identify are true surface absorption features and not artifacts of data processing methods. In all cases, a variety of different denominator ROIs were used in the ratio process to ensure that the features were not simply artifacts of a poorly-chosen denominator ROI. The final ROIs used for the spectral ratios are presented below in Figures A6 and A8). In addition, overlapping CRISM observations were examined when possible to verify the spectral features were associated with surface materials (e.g., Figure A6).The numerator and denominator spectra commonly consisted of hundreds or thousands of pixels.

Spectral ratios derived from CRISM data using the techniques described above are consistent with Fe/Mg-bearing clays minerals (Figures A6-A8). Minerals such as nontronite and saponite (Fe-smectite and Mg-smectite, respectively) exhibit Fe-OH and Mg-OH vibrational absorption features with minima near 2.28-2.29 μm and 2.30-2.32 μm, respectively, and often a weaker feature near ~2.4 μm. Mixed-layer clays such as corrensite (a 1:1 interstratified chlorite/smectite) tend to exhibit a more asymmetric spectral shape in the ~2.3-2.4 μm region due to a relative increase in the absorption near ~2.31 μm and a relative decrease in the absorption near ~2.4 μm (Figure A8). Some spectral ratios associated with preserved bedforms are consistent with Fe/Mg smectites such as nontronite and saponite (cyan spectrum in Figure A8 and red spectrum in Figure 4b in main text). Spectral ratios from other nearby deposits and preserved bedforms exhibit an asymmetry in the 2.3-2.4 μm region that may be more consistent with mixed-layer clays (e.g., chlorite/smectite), such as the example in Figure 4d. Note that the spectra presented in Figure A6 are for the same region shown in Figure 3d. As discussed in the main text, the spatial resolution of CRISM does not allow for determination of whether these clays are in the sandstones (preserved bedforms) themselves or in thin, eroded remnants of overlying strata. The clay mineral signatures observed in the bedforms along northern Mt. Sharp (Figure 4a,b) have been observed in multiple CRISM FRT and HRL images, those observed in the bedforms along western Mt. Sharp have been observed in two CRISM FRT images (Figure A6), and those associated with bedforms along the southern margin of Mt. Sharp have been observed in lower spectral/spatial resolution CRISM 'mapping' mode data (Figure A7) as well as a single CRISM FRT image (Figure A8). These consistent detections increase our confidence that the observed spectral features are associated with surface deposits and that they are indicative of Fe/Mg clay minerals.

References

Grotzinger, J.P. et al. (2005), Stratigraphy and sedimentology of a dry to wet eolian depositional system, Burns formation, Meridiani Planum, Earth and Planetary Science Letters, 240, 11-72.

Milliken, R.E., J.P. Grotzinger and B.J. Thomson (2010), Paleoclimate of Mars as captured by the stratigraphic record in Gale Crater, GRL, 37, L04201.

Murchie, S. et al. (2009), Compact Reconnaissance Imaging Spectrometer for Mars investigation and data set from the Mars Reconnaissance Orbiter's primary science phase, J. Geophys. Res., 114, E00D07.

Okubo, C.H. and A.S. McEwen (2007), Fracture-controlled paleo-fluid flow in Candor Chasma, Mars, Science, 315, 938-985.

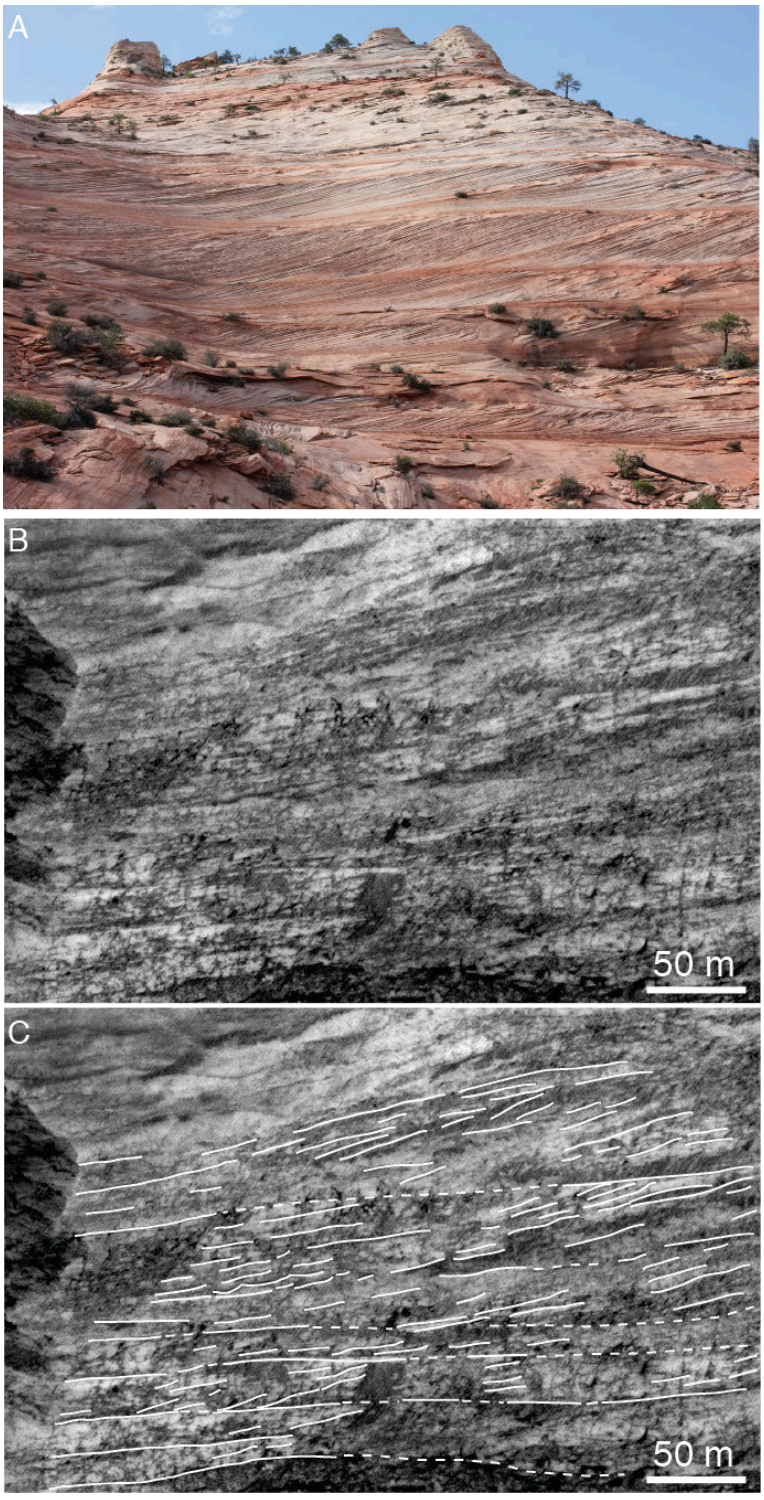

Figure A1. Comparison of eolian sandstones on Earth and inferred eolian sandstones on Mars. (a) Navajo sandstone in Zion National Park, Utah, USA; (b) & (c) strata exposed in Lower Mt. Sharp, same as Figures 1c,d in main text. Note similarity in hierarchy of bounding surfaces and low-angle stratification between terrestrial and Martian examples.

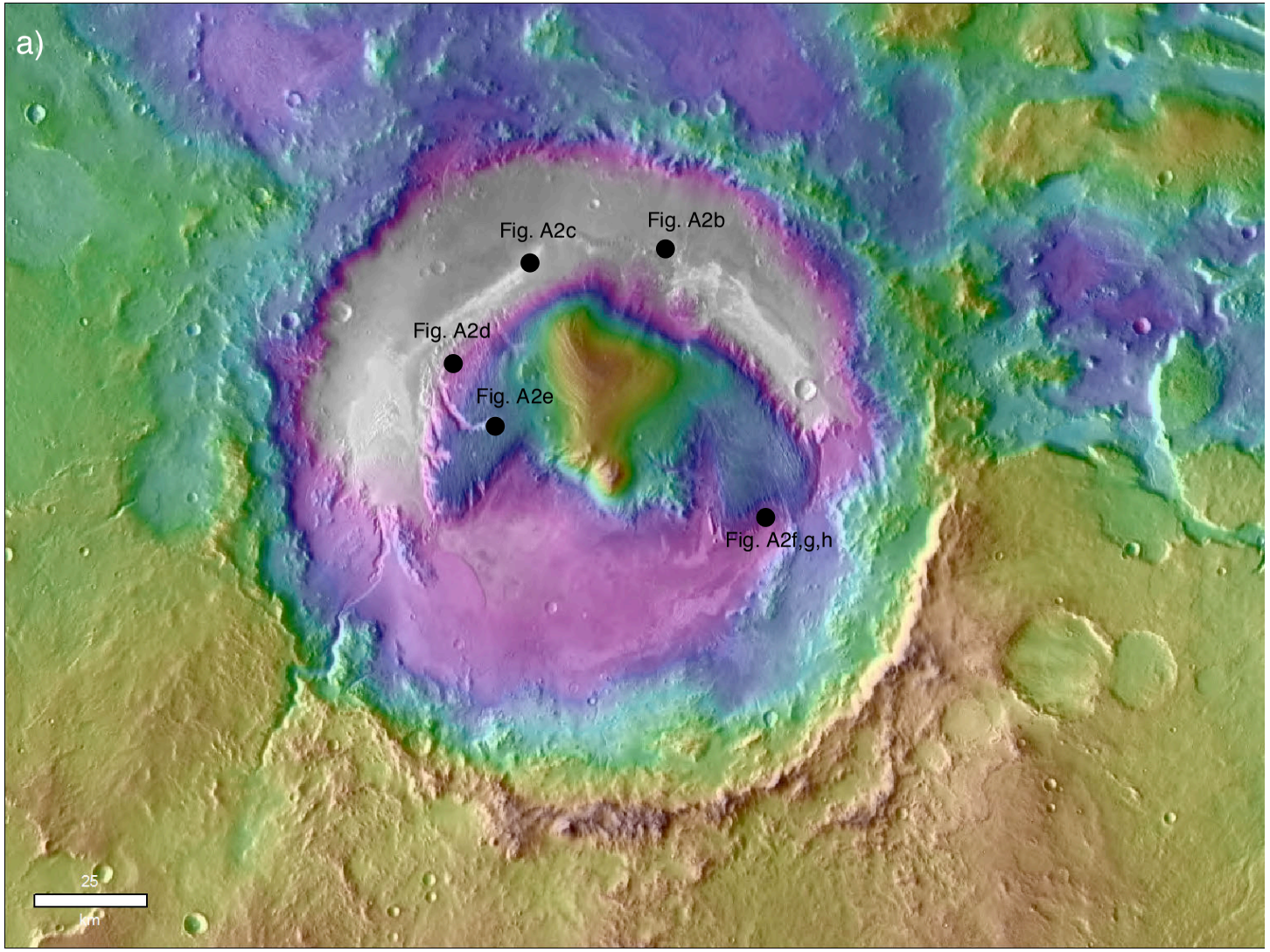

Figure A2. Locations and examples of filled fractures and possible recrystallization zones indicating post-depositional fluid flow in the Lower fm. of Mt. Sharp. (a) MOLA topographic map on THEMIS daytime infrared mosaic of Gale Crater. Black dots indicate locations of best examples of filled fractures on the crater floor and in the Lower fm. of Mt. Sharp.

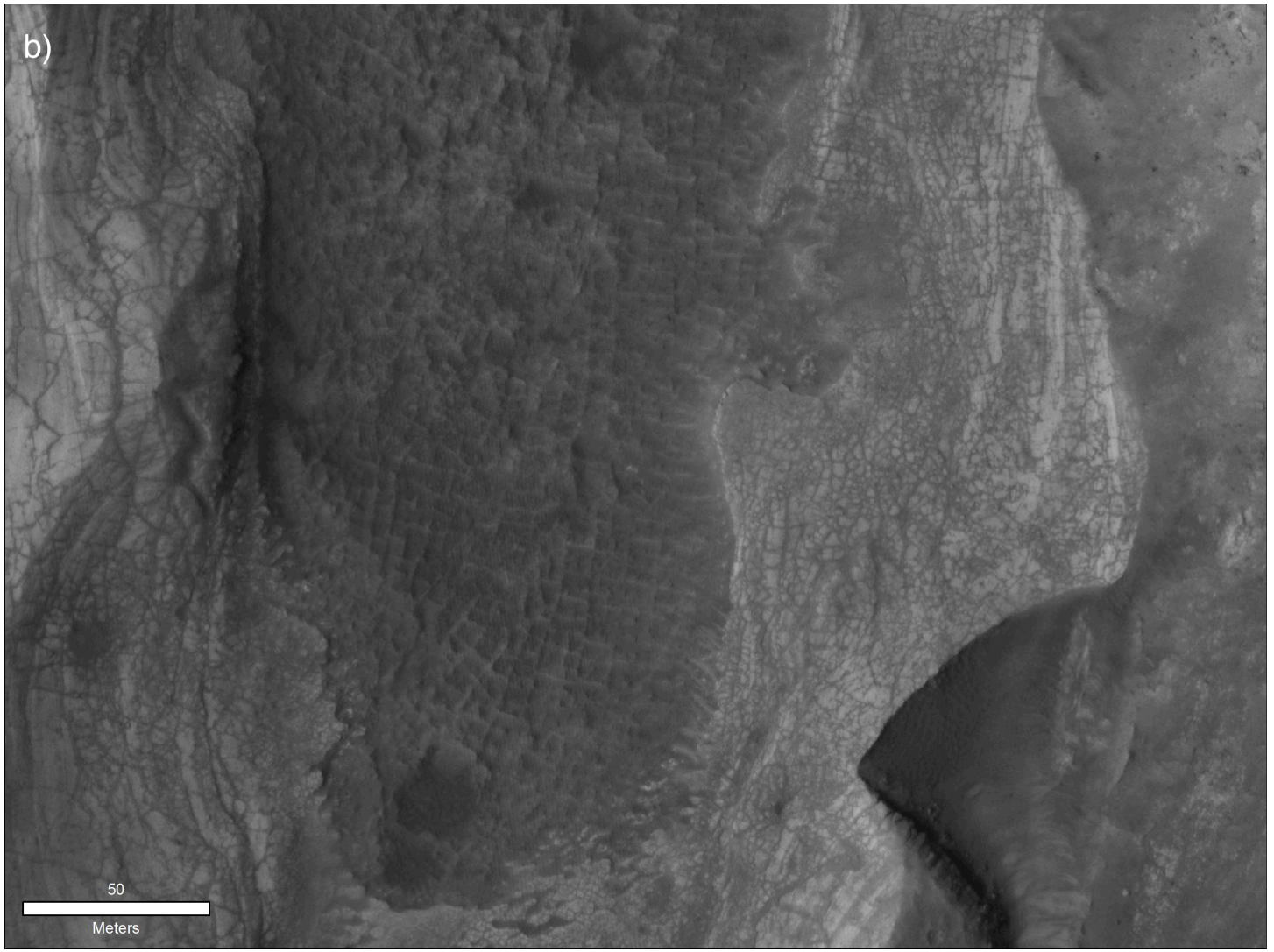

Figure A2, cont. (b) Example of complex, box-like network of filled fractures in NE portion of lowermost strata in Lower fm. of Mt. Sharp. See Figure A2a for location.

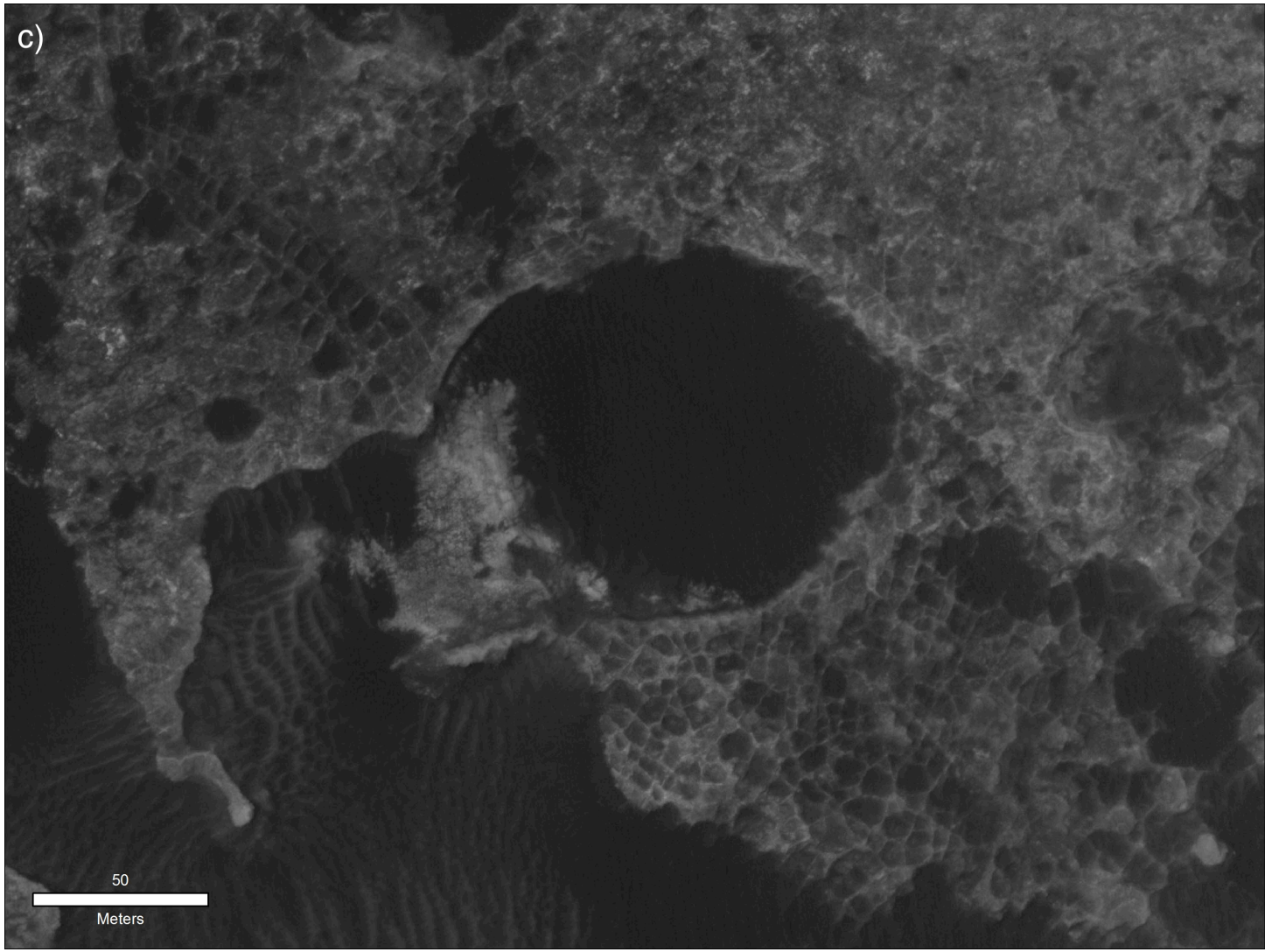

Figure A2, cont. (c) Example of complex network of filled fractures in NW portion of lowermost strata in Lower fm. of Mt. Sharp. See Figure A2a for location.

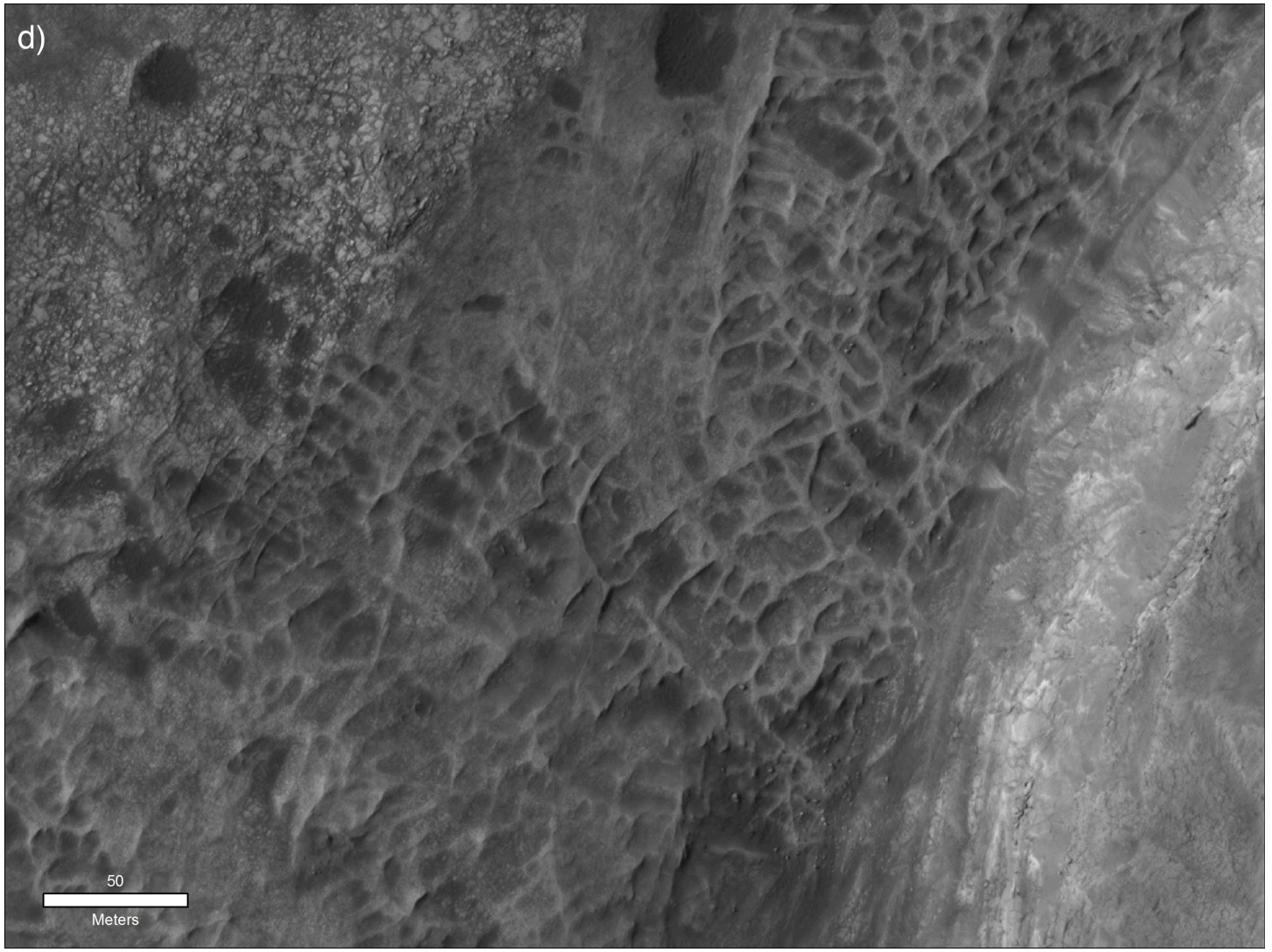

Figure A2, cont. (d) Example of complex network of filled fractures in NW portion of Lower fm. of Mt. Sharp as shown in Fig. 22 of *Anderson and Bell* [2010]. See Figure A2a for location.

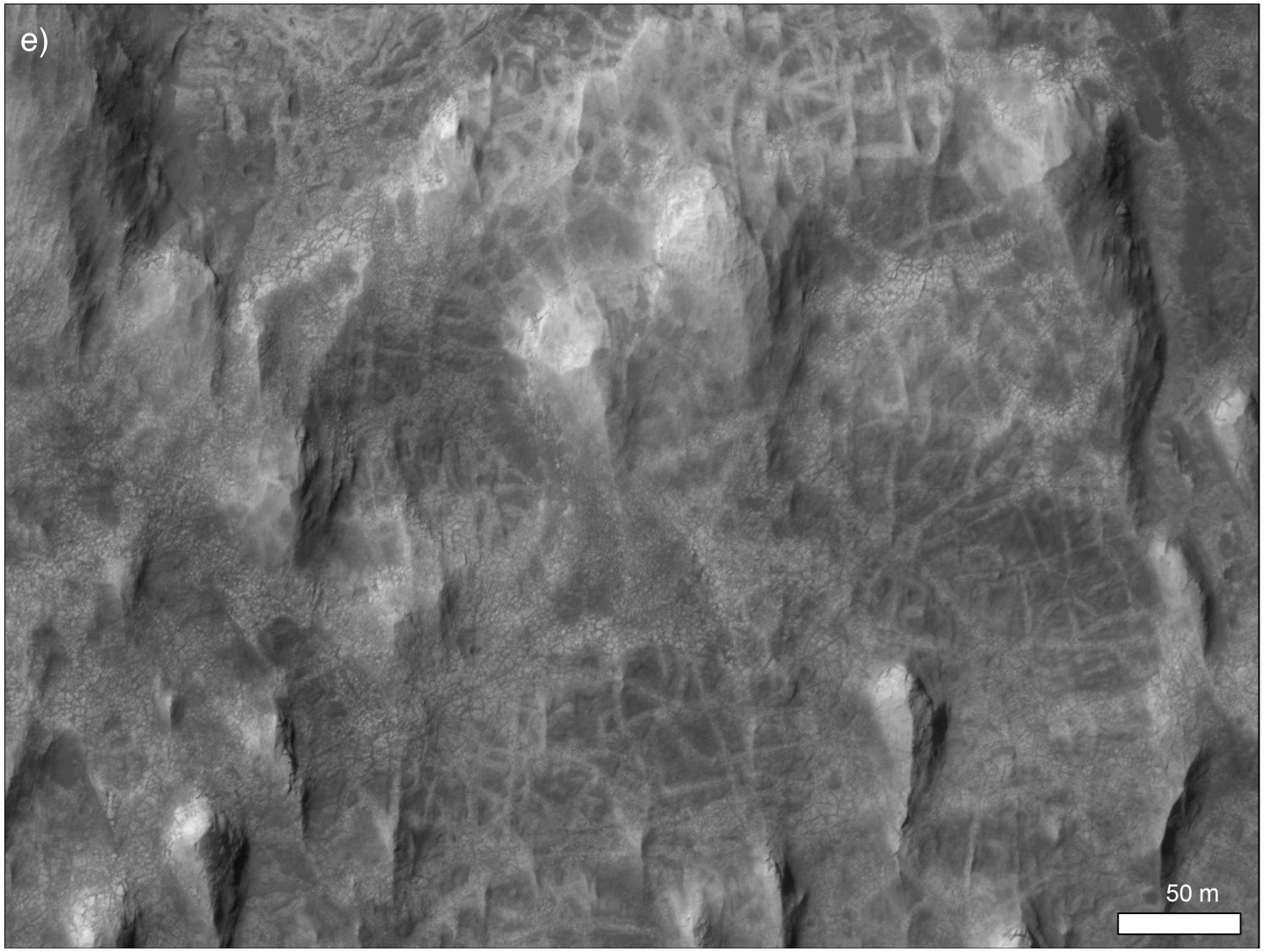

Figure A2, cont. (e) Example of complex network of filled fractures in NW portion of Lower fm. of Mt. Sharp similar to Fig. 20 of *Anderson and Bell* [2010]. See Figure A2a for location.

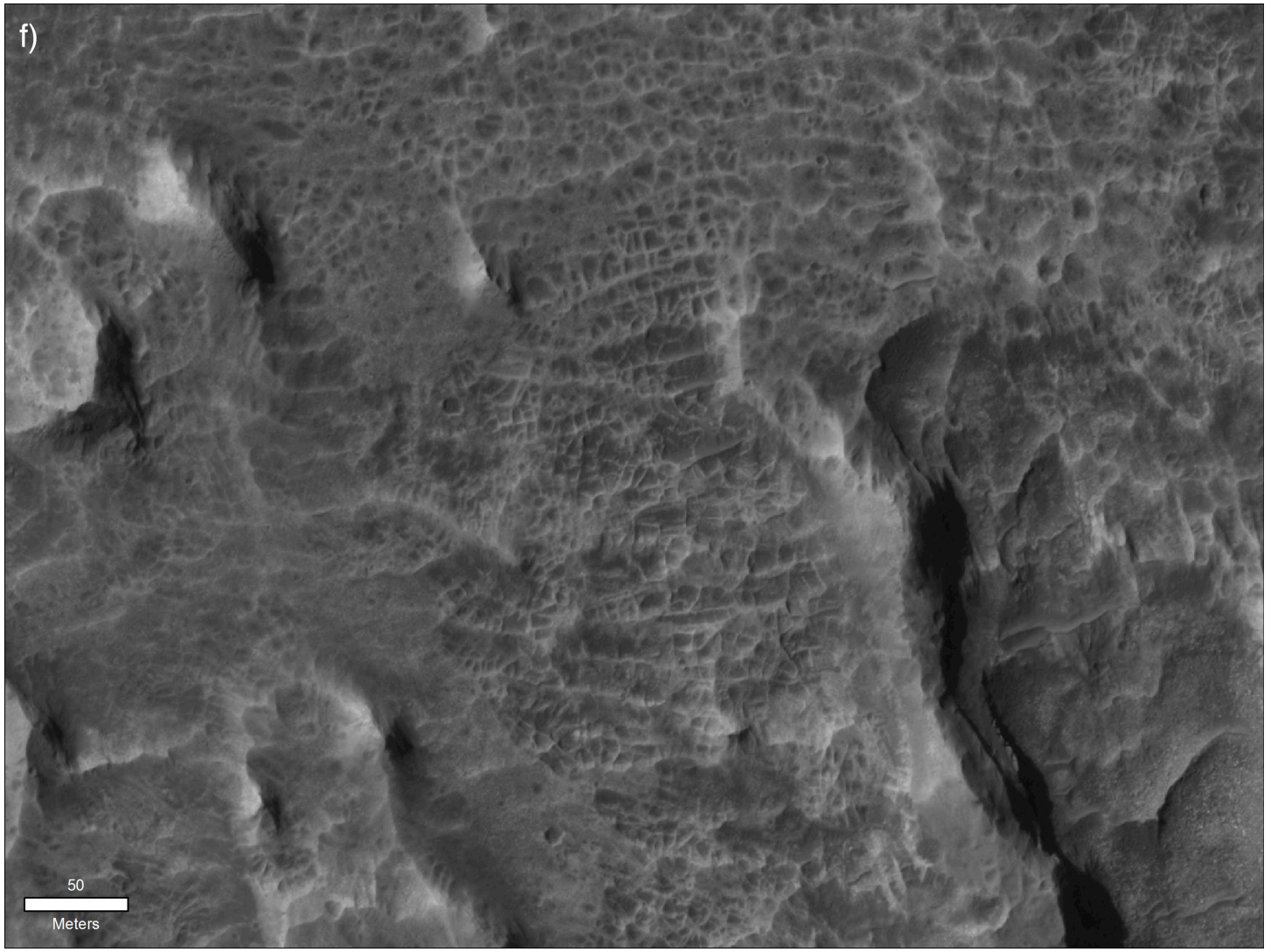

Figure A2, cont. (f) Example of complex network of filled fractures in SE portion of Lower fm. of Mt. Sharp. Note similarities to previous examples (Figure A2d,e) which were in the NW portion of Mt. Sharp. See Figure A2a for location.

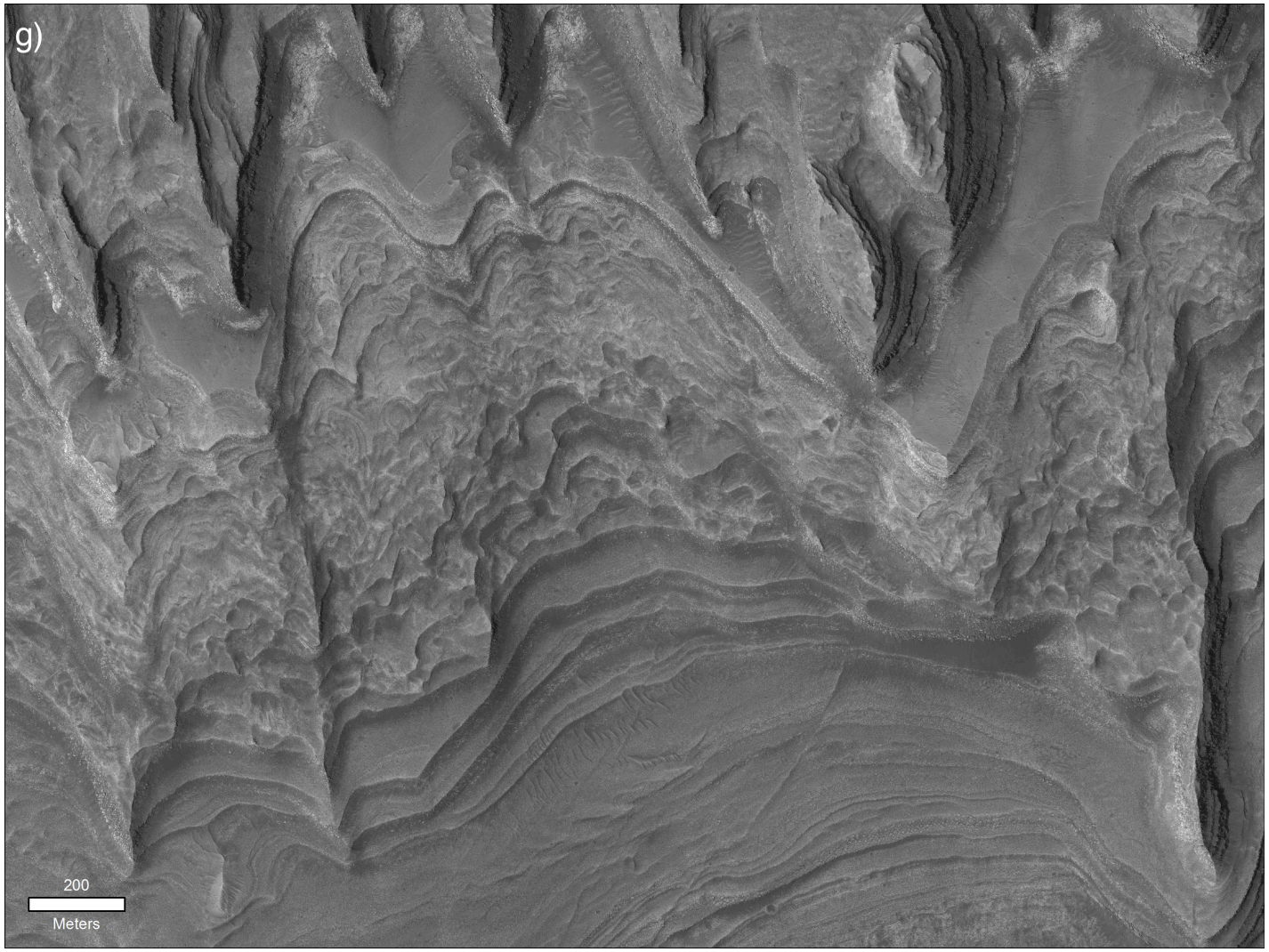

Figure A2, cont. (g) Potential recrystallization zone in the Lower fm. of Mt. Sharp. Note the contrast between the well-defined, parallel bedding in the upper and lower portions of the image and the highly irregular, non-planar zone in the middle of the image. The poorly defined bedding in the central portion may be the result of dissolution and re-precipitation of soluble salts. See supporting material text for discussion and Figure A2a for location.

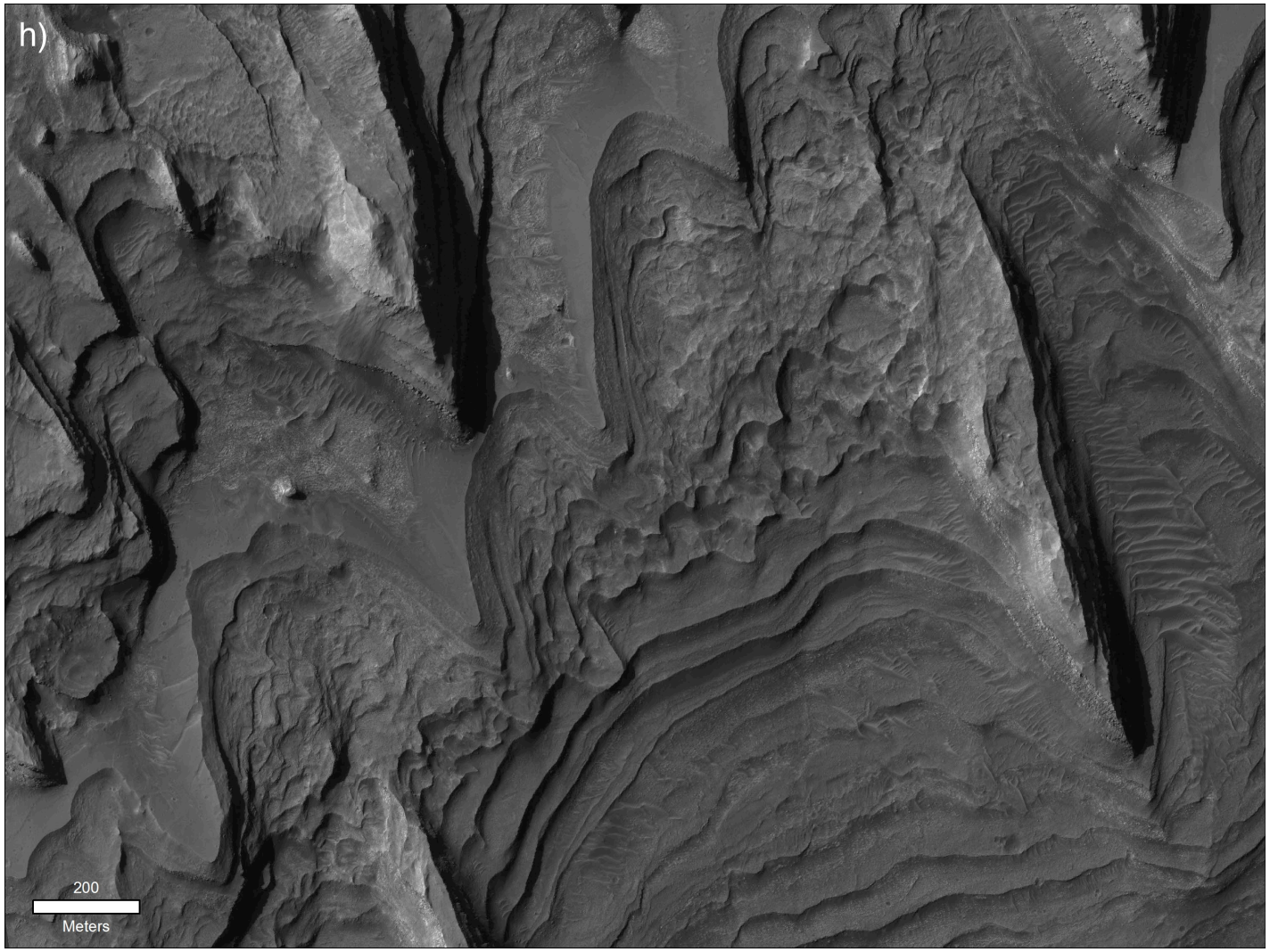

Figure A2, cont. (h) Potential recrystallization zone in the Lower fm. of Mt. Sharp. Note the contrast between the well-defined, parallel bedding in the upper and lower portions of the image and the highly irregular, non-planar zone in the middle of the image. The poorly defined bedding in the central portion may be the result of dissolution and re-precipitation of soluble salts. See supporting material text for discussion and Figure A2a for location.

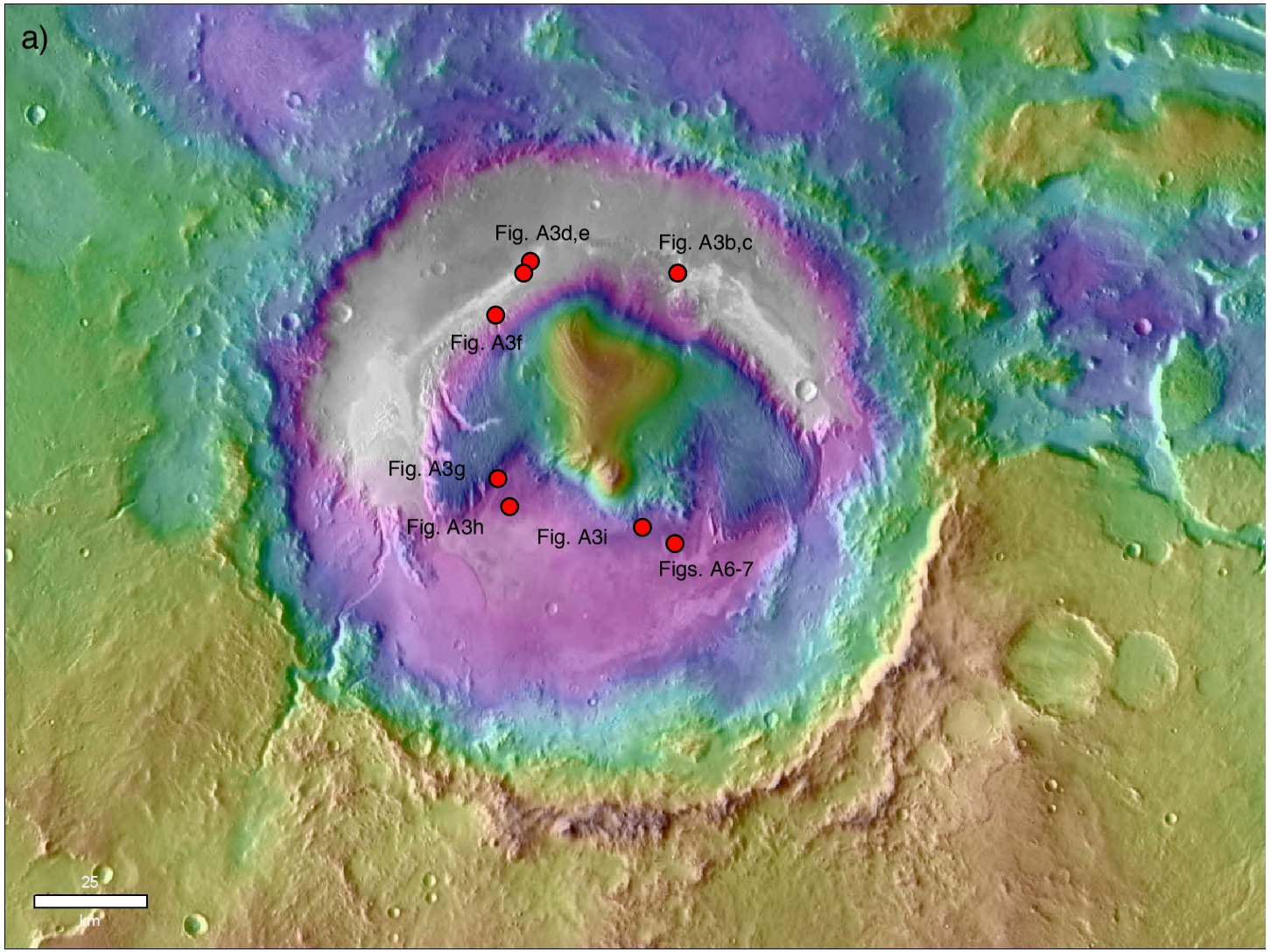

Figure A3. Locations and examples of preserved bedforms in Gale Crater. (a) MOLA topographic map on THEMIS daytime infrared mosaic of Gale Crater. Red dots indicate locations of best examples of preserved bedforms on the crater floor and in the Lower fm. of Mt. Sharp.

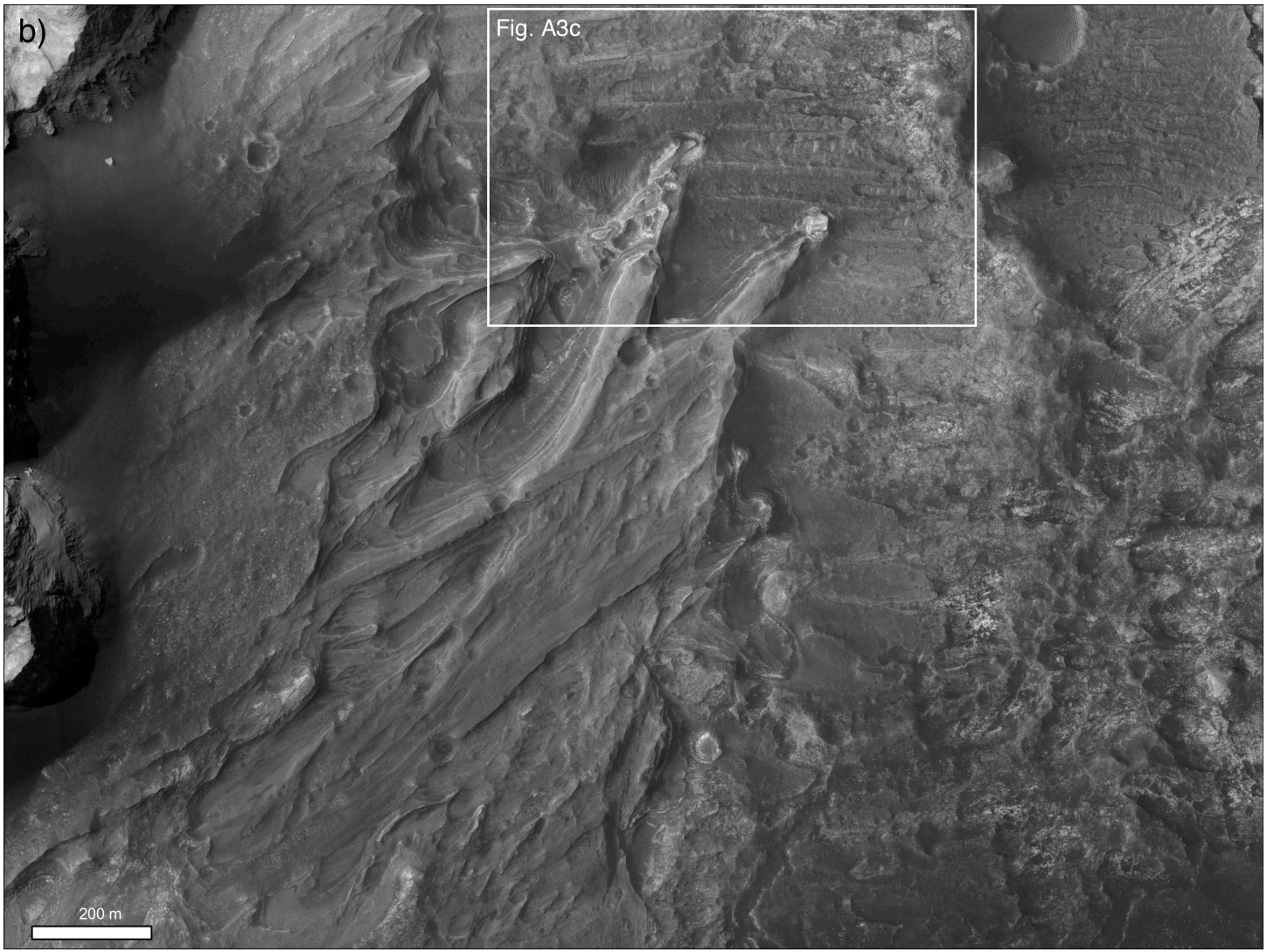

Figure A3, cont. (b) Example of raised, linear features consistent with preserved bedforms (dunes) in NE portion of Mt. sharp. These E-W trending linear features are overlain by inverted and intertwined channel deposits, as well as a breccia unit (dark unit in leftmost portion of image that contains meter-sized white clasts). Figure A3c shows a closeup as indicated by the region outlined in the white box. See Figure A3a for location.

Figure A3, cont. (c) Example of raised, linear features consistent with preserved bedforms (dunes) in NE portion of Mt. sharp. Note that features appear to be exposed as overlying sediments are eroded, consistent with burial of the dunes by the overlying fluvial deposits (channels in positive relief). See Figure A3a for location.

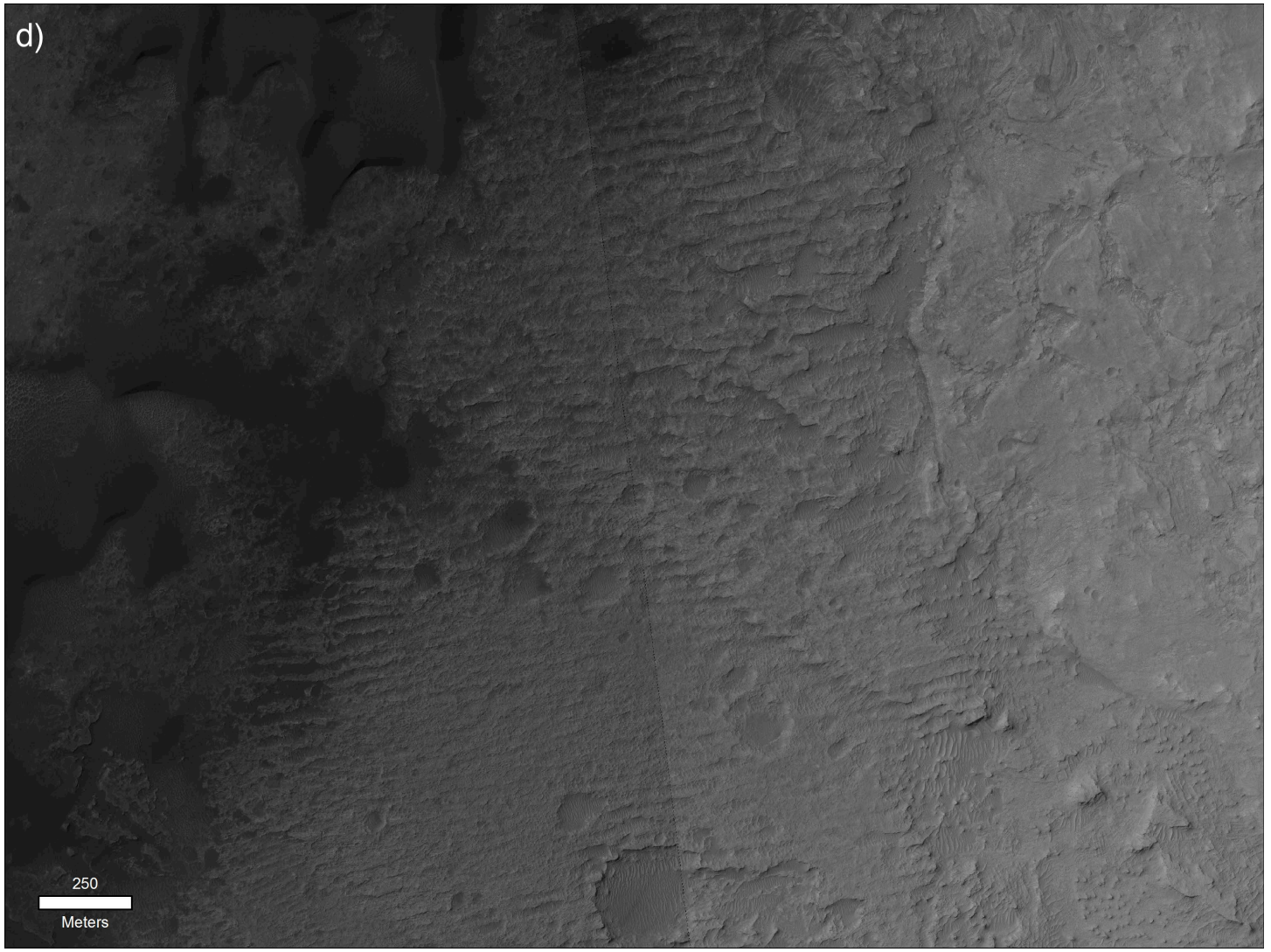

Figure A3, cont. (d) Example of raised, linear features consistent with preserved bedforms (dunes) in Gale Crater. This unit has a 'washboard' morphology and is part of the 'mound skirting unit' mapped by *Anderson and Bell* [2010]. See Figure A3a for location.

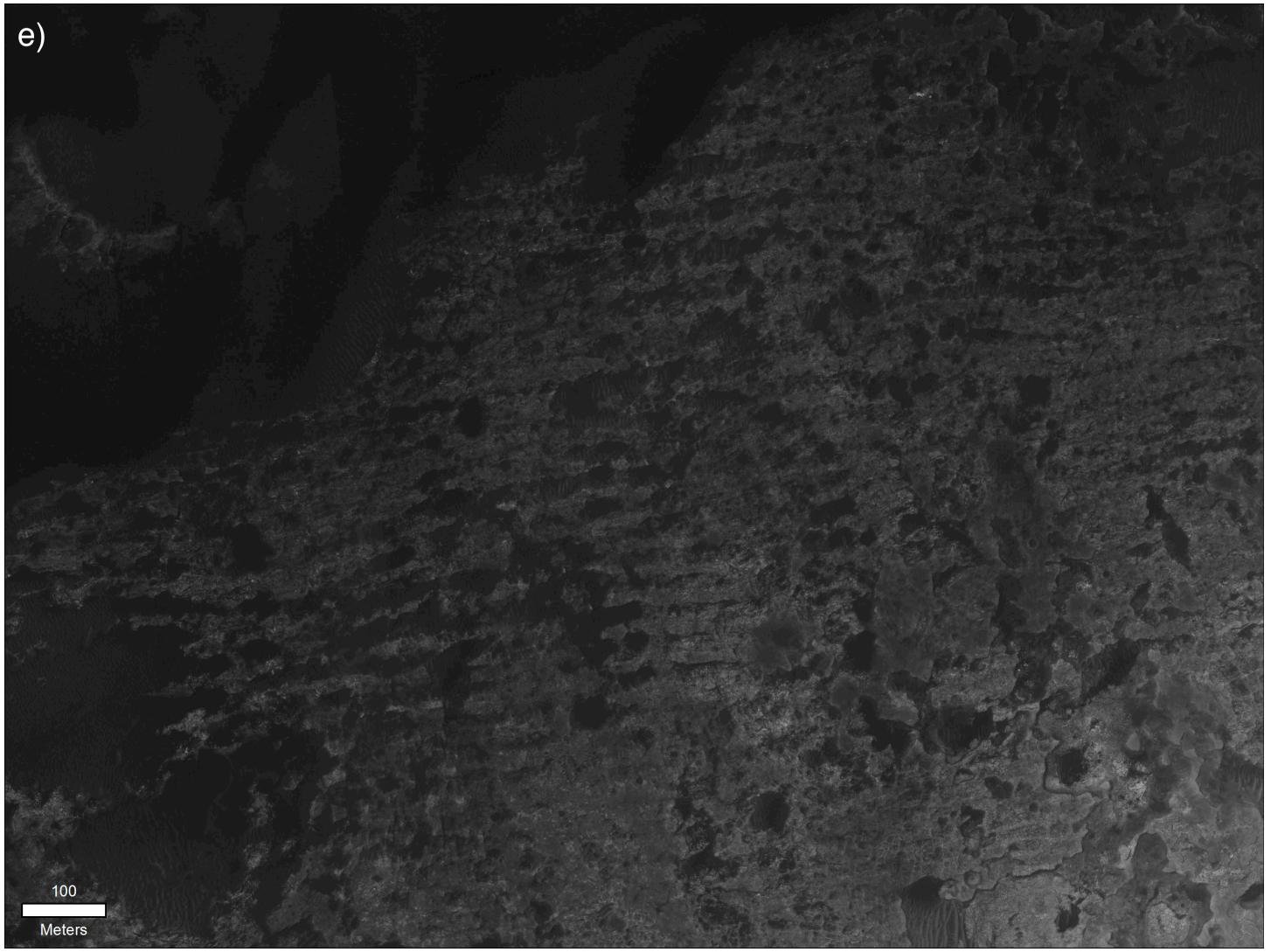

Figure A3, cont. (e) Example of raised, linear features consistent with preserved bedforms (dunes) in Gale Crater. This unit has a 'washboard' morphology and is part of the 'mound skirting unit' mapped by *Anderson and Bell* [2010]. See Figure A3a for location.

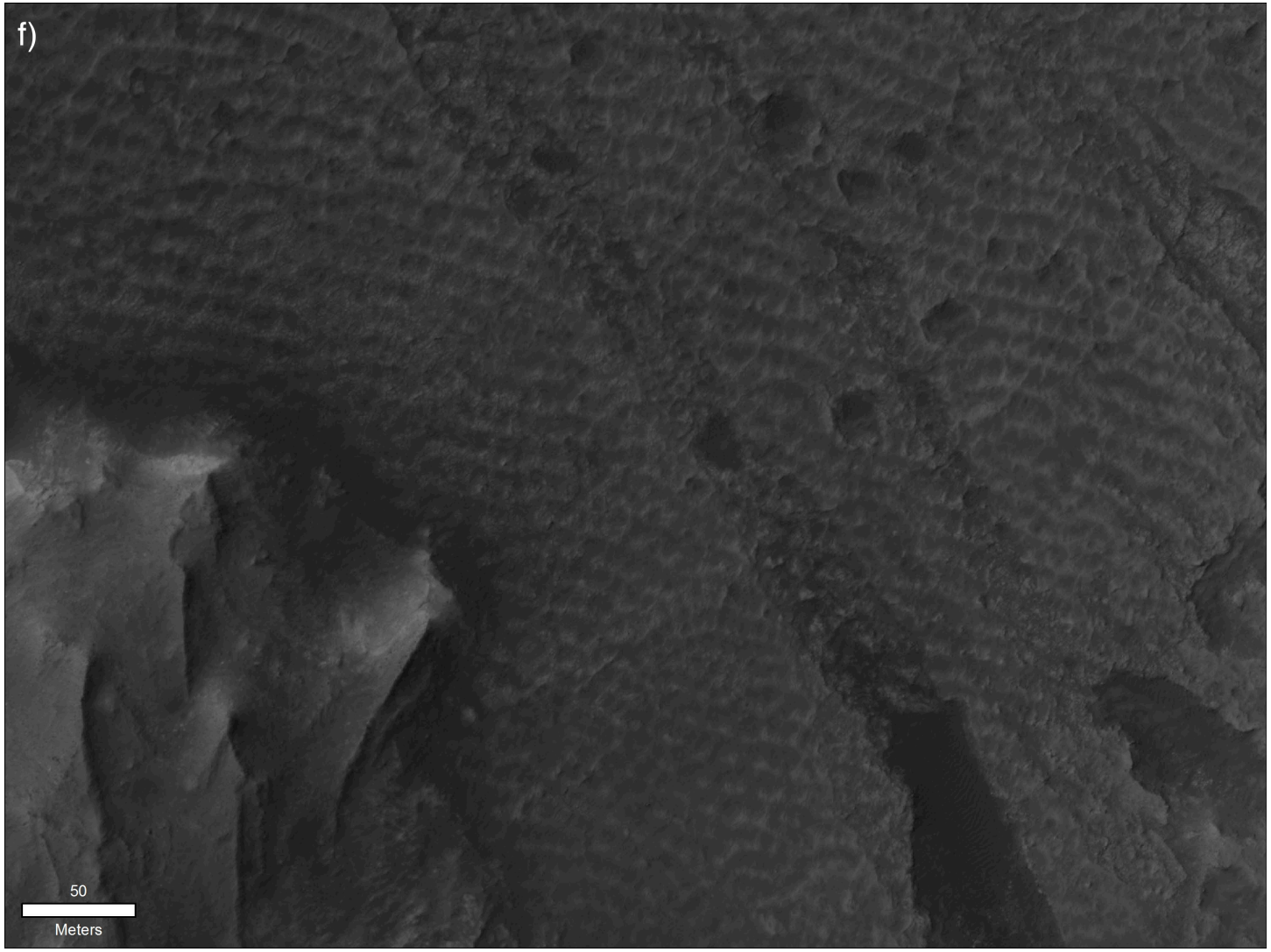

Figure A3, cont. (f) Example of raised, intersecting features consistent with preserved bedforms (dunes) in Gale Crater. Unlike the 'washboard' morphology in the previous examples, these features indicate an interference pattern suggestive of transport from multiple directions. See Figure A3a for location.

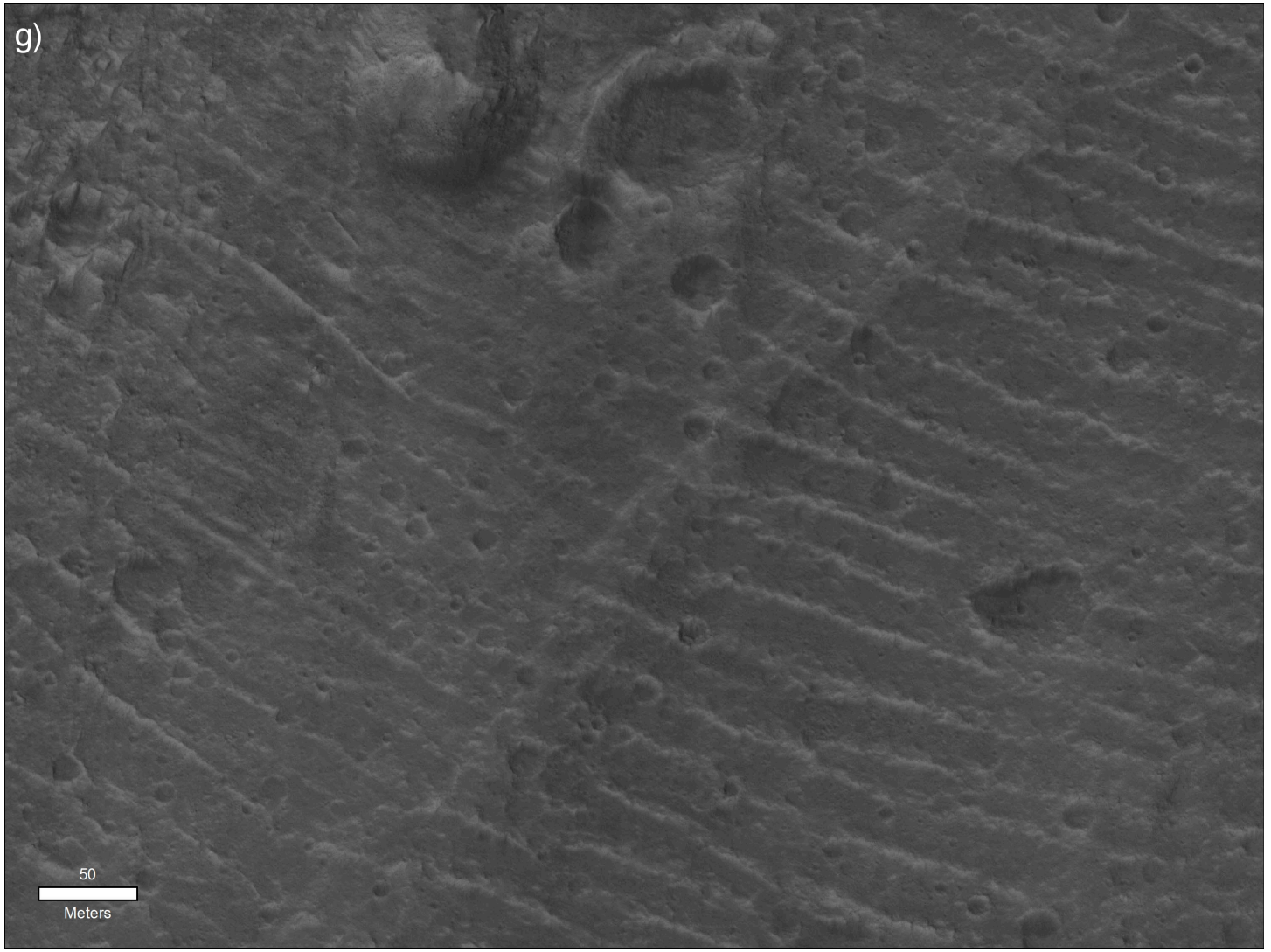

Figure A3, cont. (g) Example of raised, linear features consistent with preserved bedforms (dunes) south of Mt. Sharp in Gale Crater. Unlike the flat-topped morphology of the 'washboard' unit in previous examples, these features appear to have the dune crests largely preserved, as well as crest bifurcation (white arrow). See Figure A3a for location.

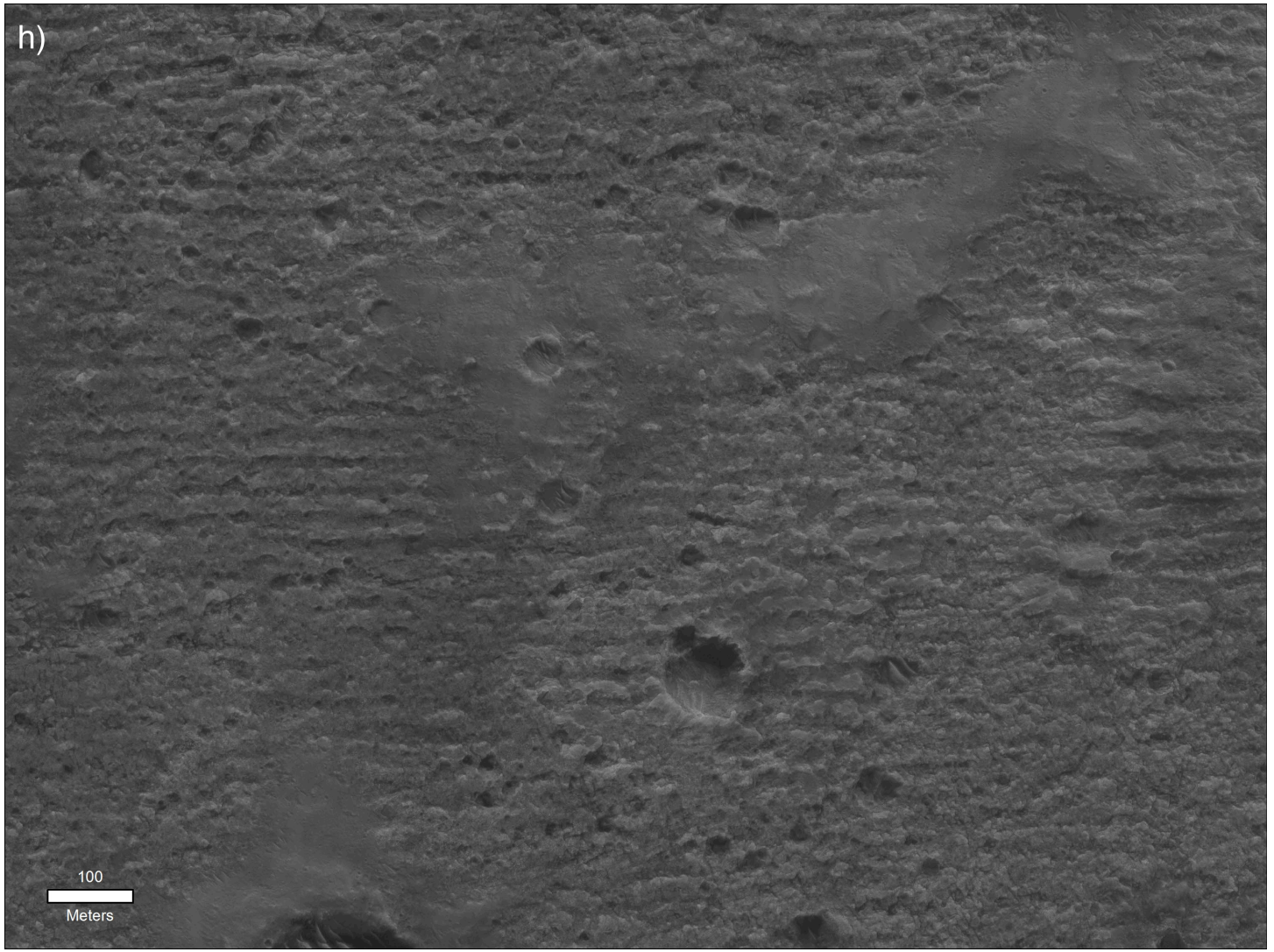

Figure A3, cont. (h) Example of flat-topped, linear features consistent with preserved bedforms (dunes). This example of 'washboard' morphology is found along the southwest margin of Mt. Sharp and is very similar to previous examples from the northern margin (e.g., Figure A3e). Here, erosion of an overlying, darker, and smoother unit appears to reveal the washboard morphology. See Figure A3a for location.

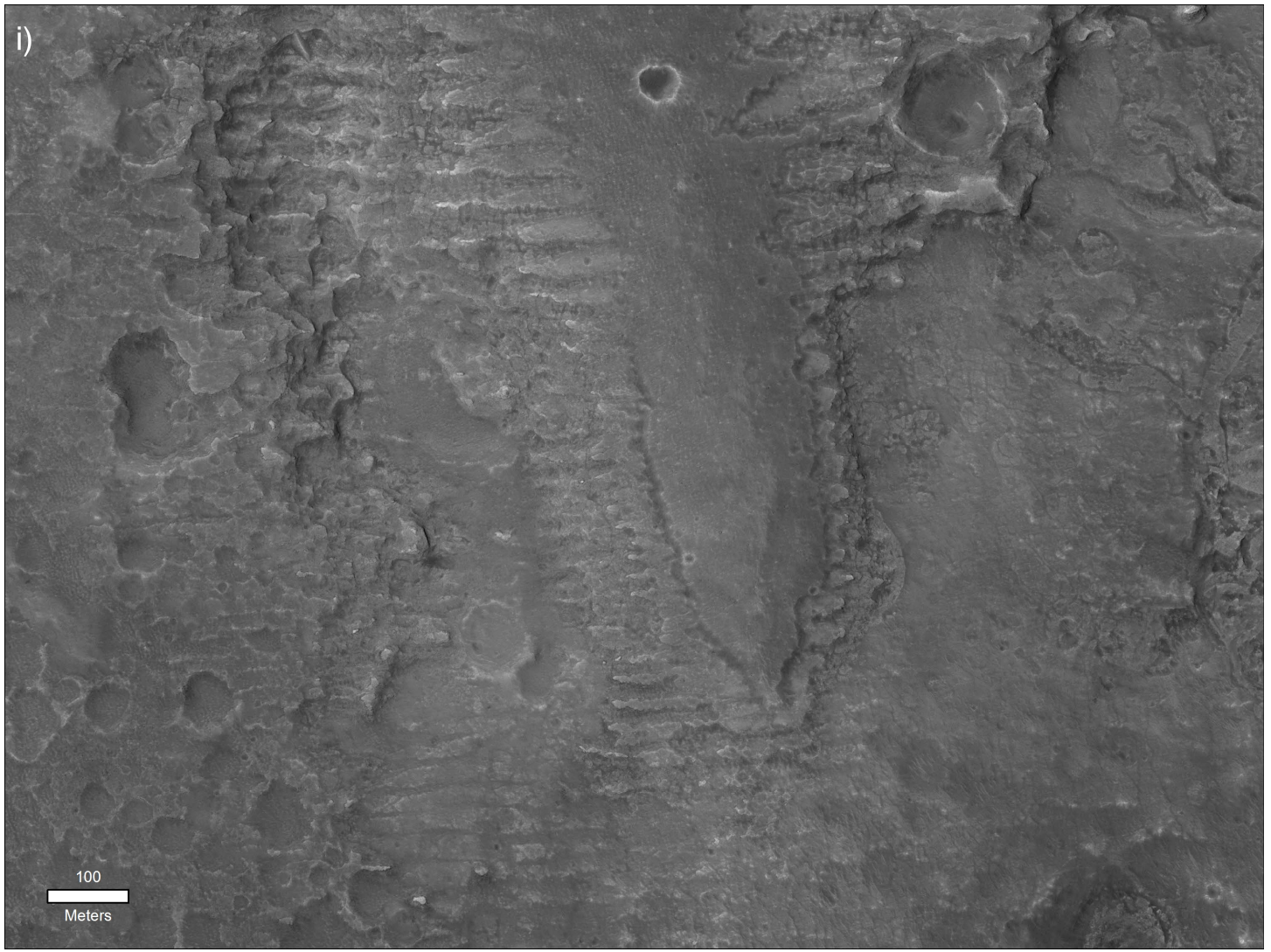

Figure A3, cont. (i) Example of possible preserved bedforms and 'washboard' morphology along the southern margin of Mt. Sharp. As in Figure A3h, erosion of an overlying, darker, and smoother unit appears to reveal the washboard morphology. Also, note that the 'washboard' texture and linear ridges are present in multiple stratigraphic units. See Figure A3a for location.

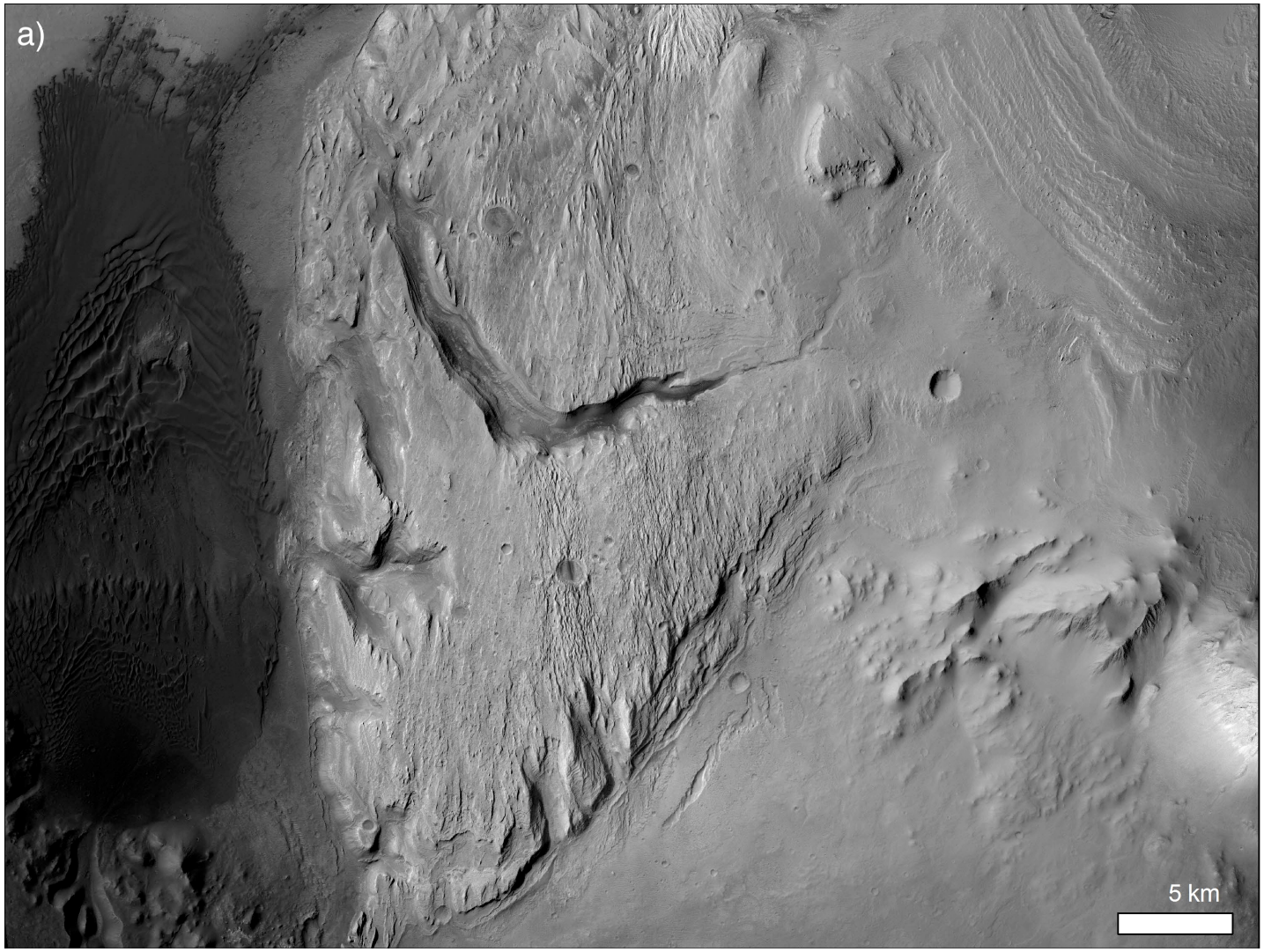

Figure A4. Examples of preserved bedforms associated with fan deposits along the southwest margin of Mt. Sharp. (a) Context Camera (CTX) mosaic of the southwestern portion of the Lower fm. of Mt. Sharp.

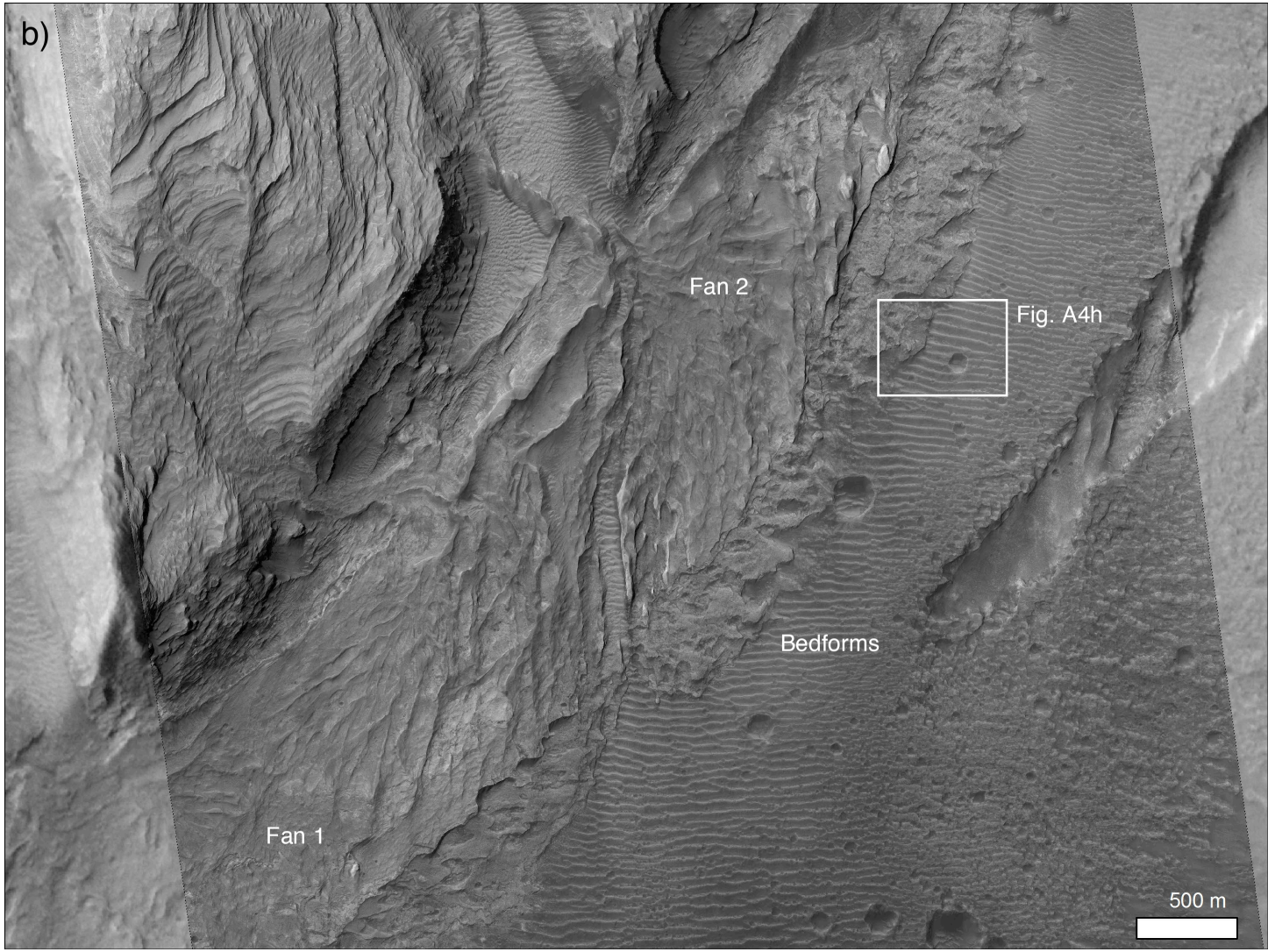

Figure A4, cont. (b) Raised, linear features that trend E-W and exhibit bifurcation are consistent with wholly preserved bedforms. These bedforms are overlain by sediments associated with fluvial incision of the Lower fm. (Fans 1 and 2). Superposition shows that the bedforms pre-date the fan deposits, and if fluvial incision of the Lower fm. pre-dates deposition of the Upper fm., then this would imply the bedforms also pre-date the Upper fm.

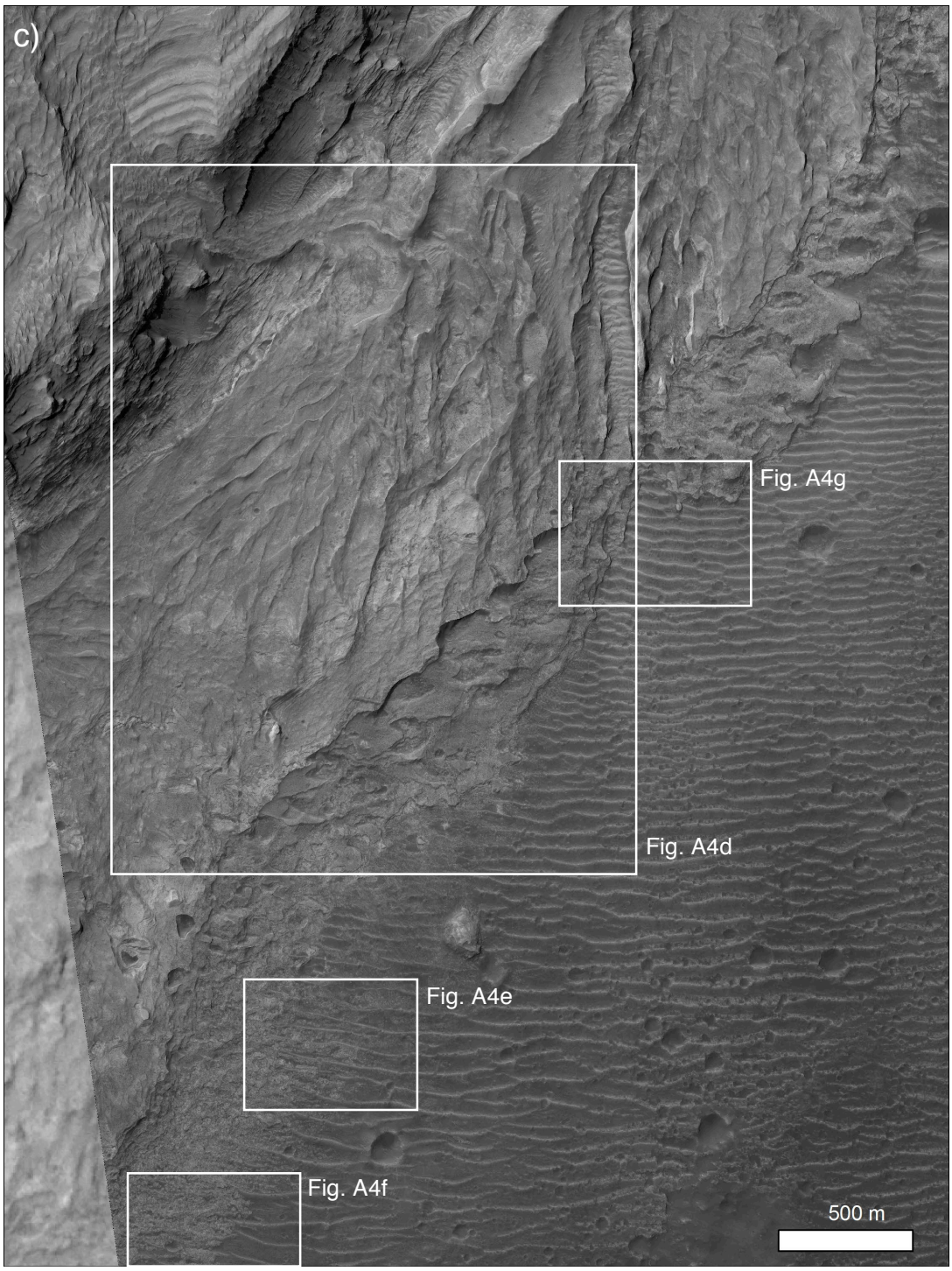

Figure A4, cont. (c) Closer view of fan deposits and bedforms shown in Figure A4b. Note the large area covered by the preserved bedforms and their abrupt termination along the contact with the fan deposits to the west (e.g., Figure A4g). Closer views of the HiRISE image indicate that the lowermost strata of the fan deposits are overlying the bedforms and fill in the interdune regions (Figures A4e,f).

Figure A4, cont. (d) Closer view of the lower fan deposit (Fan 1) and bedforms shown in Figure A4c. Note the inverted topography of the distributary system. The sediments that form these deposits are sourced from the Lower fm., and there are at least two fan systems that have developed due to this erosion (see Figure A4b). See Figure A4c for location.

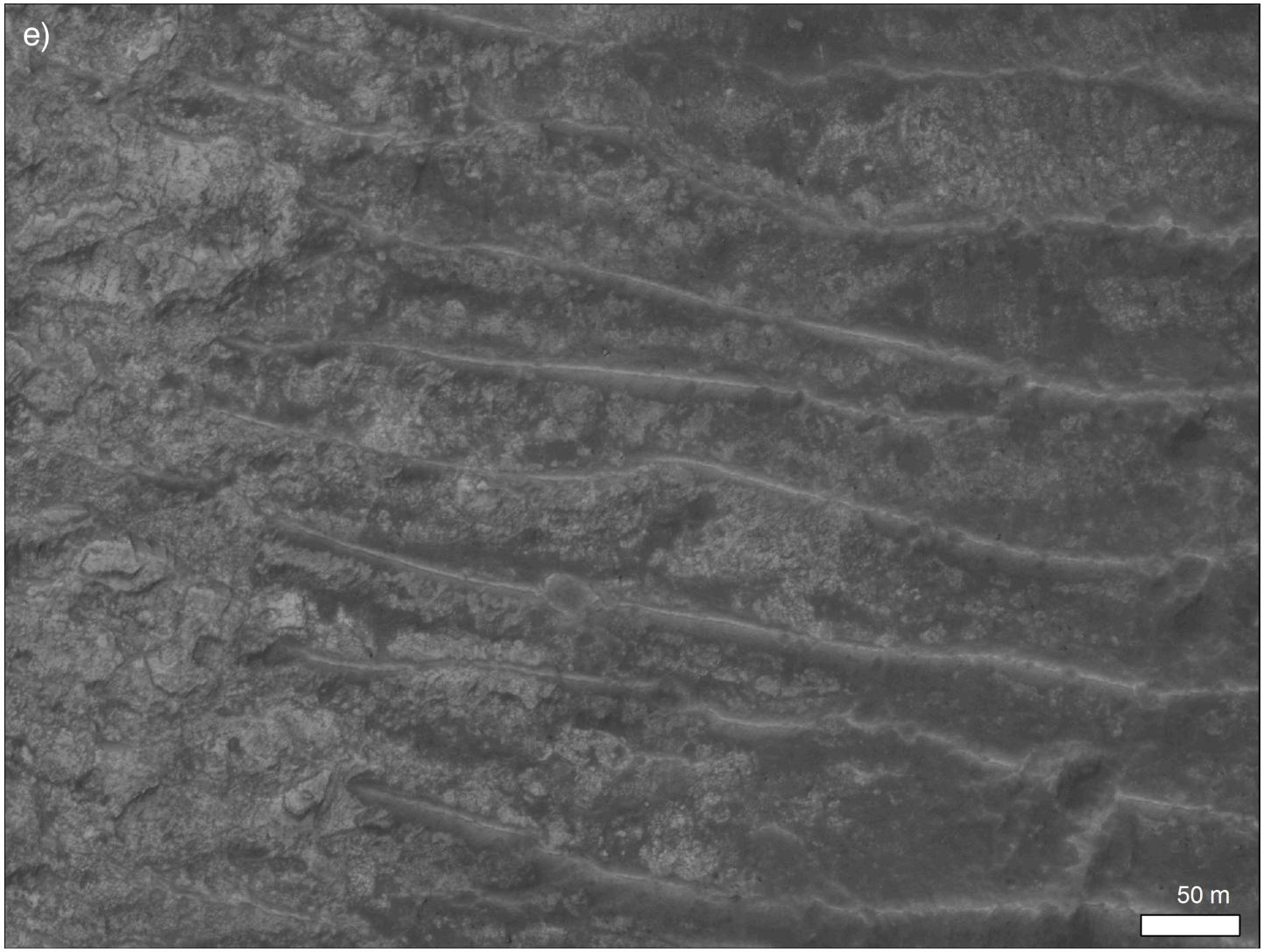

Figure A4, cont. (e) Close-up view showing that lowermost strata in Fan 1 superpose the preserved bedforms. Note how the lighter-toned sediments fill in the interdune regions and, as they are eroded back, the crests are preferentially exposed. Also, note the ability of the bedforms to retain impact craters, showing that they are at least partially lithified. Exquisite preservation of original dune topography such as this is rare on Earth and requires specific conditions, including early cementation and rapid burial. See Figure A4c for location.

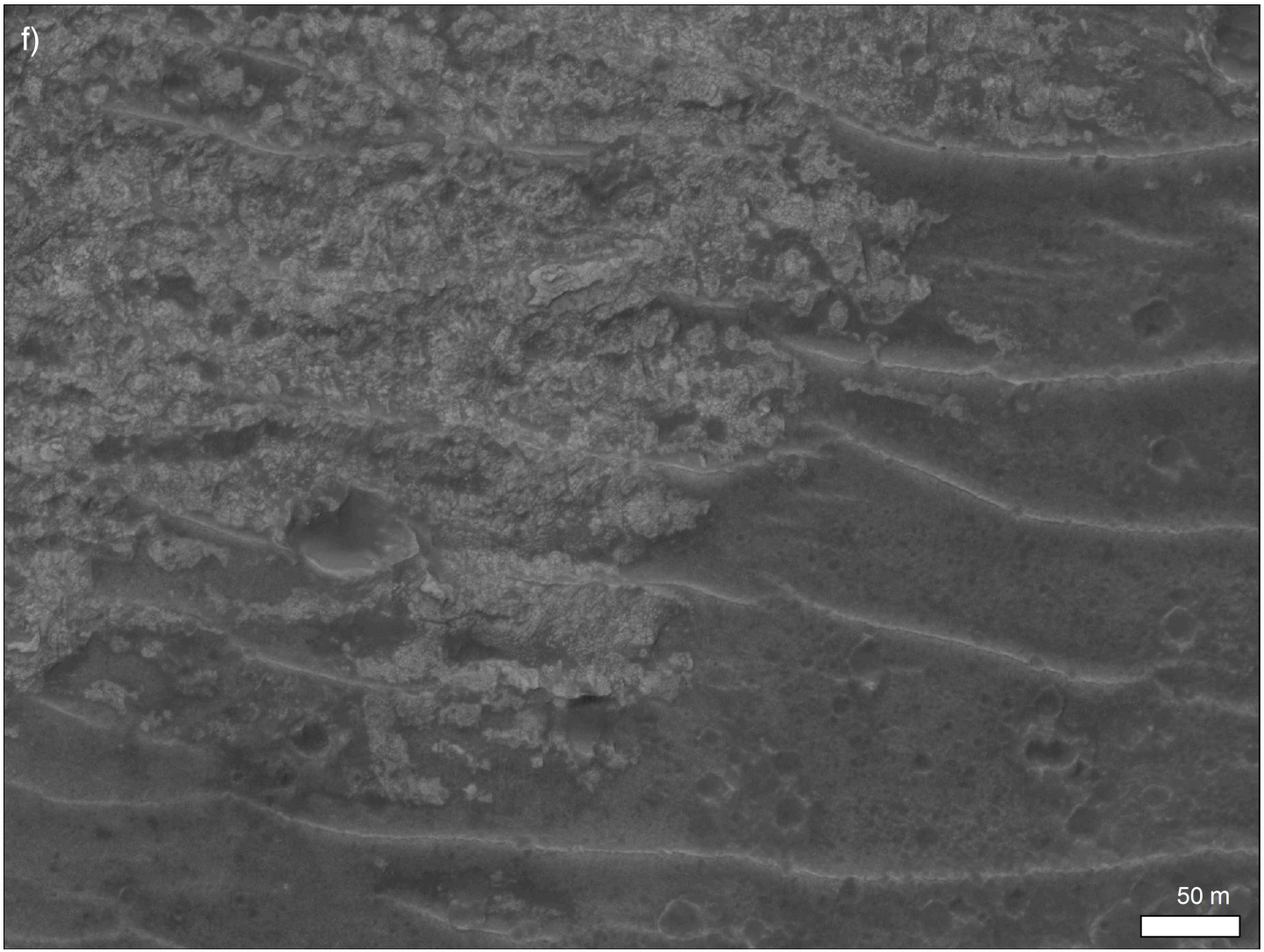

Figure A4, cont. (f) Close-up view showing that lowermost strata in Fan 1 superpose the preserved bedforms. Note how the lighter-toned sediments fill in the interdune regions and, as they are eroded back, the crests are preferentially exposed. Also, note the ability of the bedforms to retain impact craters, showing that they are at least partially lithified. Exquisite preservation of original dune topography such as this is rare on Earth and requires specific conditions, including early cementation and rapid burial. See Figure A4c for location.

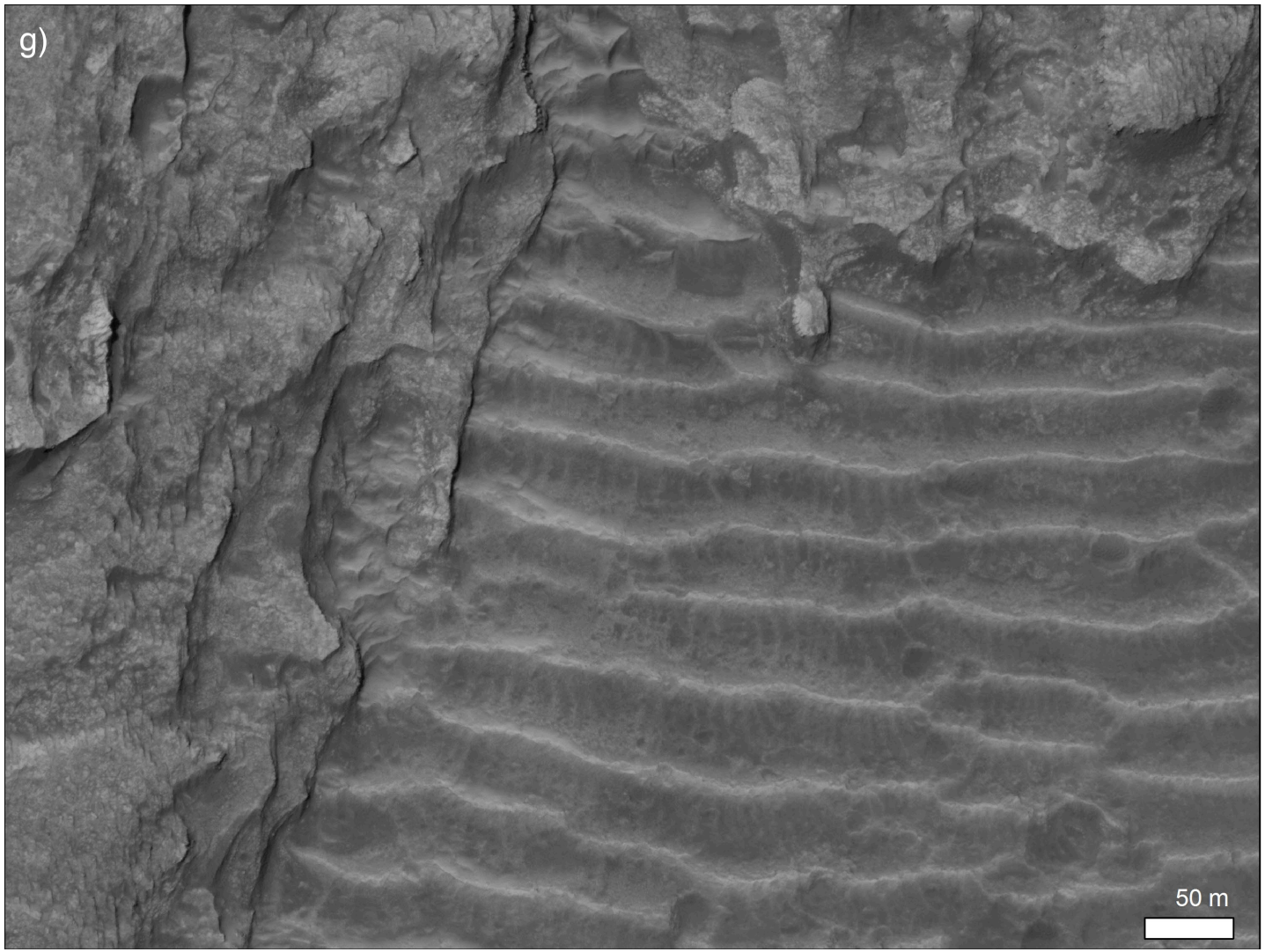

Figure A4, cont. (g) Close-up view showing preserved bedforms that underlie fan deposits along southern Mt. Sharp. Note the abrupt termination and lack of deflection of the ridges (dune crests) along the western contact with the fan deposits; this is consistent with the the fan deposits superposing the bedforms (see Figures A4e,f). In addition to exhibiting bifurcation, the preserved bedforms appear to exhibit 'ladderback' bedforms orthogonal to the direction of the primary features. See Figure A4c for location.

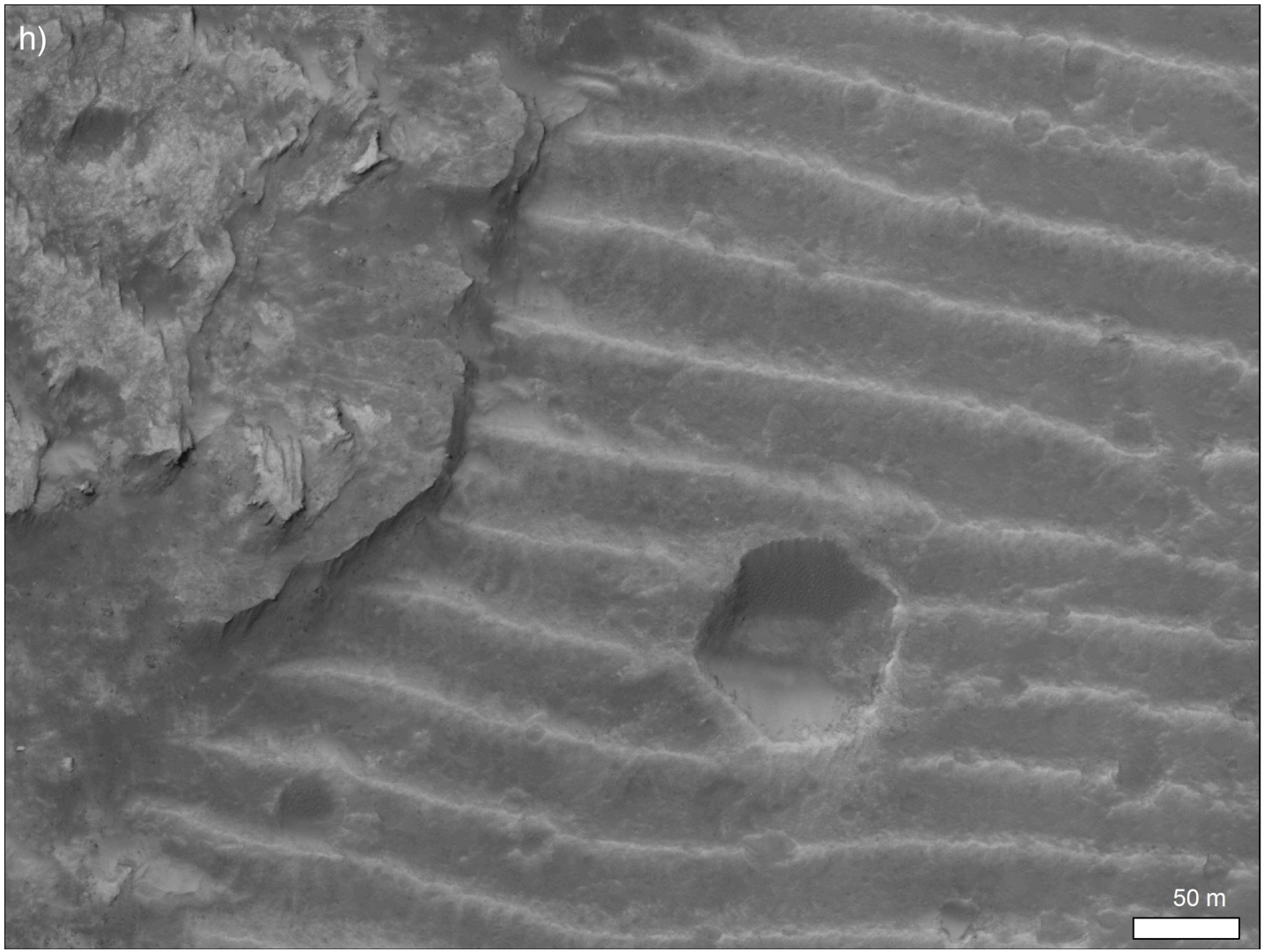

Figure A4 cont. (h) Close-up view showing preserved bedforms that underlie fan deposits along southern Mt. Sharp. Note the abrupt termination and lack of deflection of the ridges (dune crests) along the western contact with the fan deposits; this is consistent with the the fan deposits superposing the bedforms (see Figures A4e,f). Note the remarkably straight crests of the bedforms and their ability to retain craters, consistent with cementation and lithification. See Figure A4b for location.

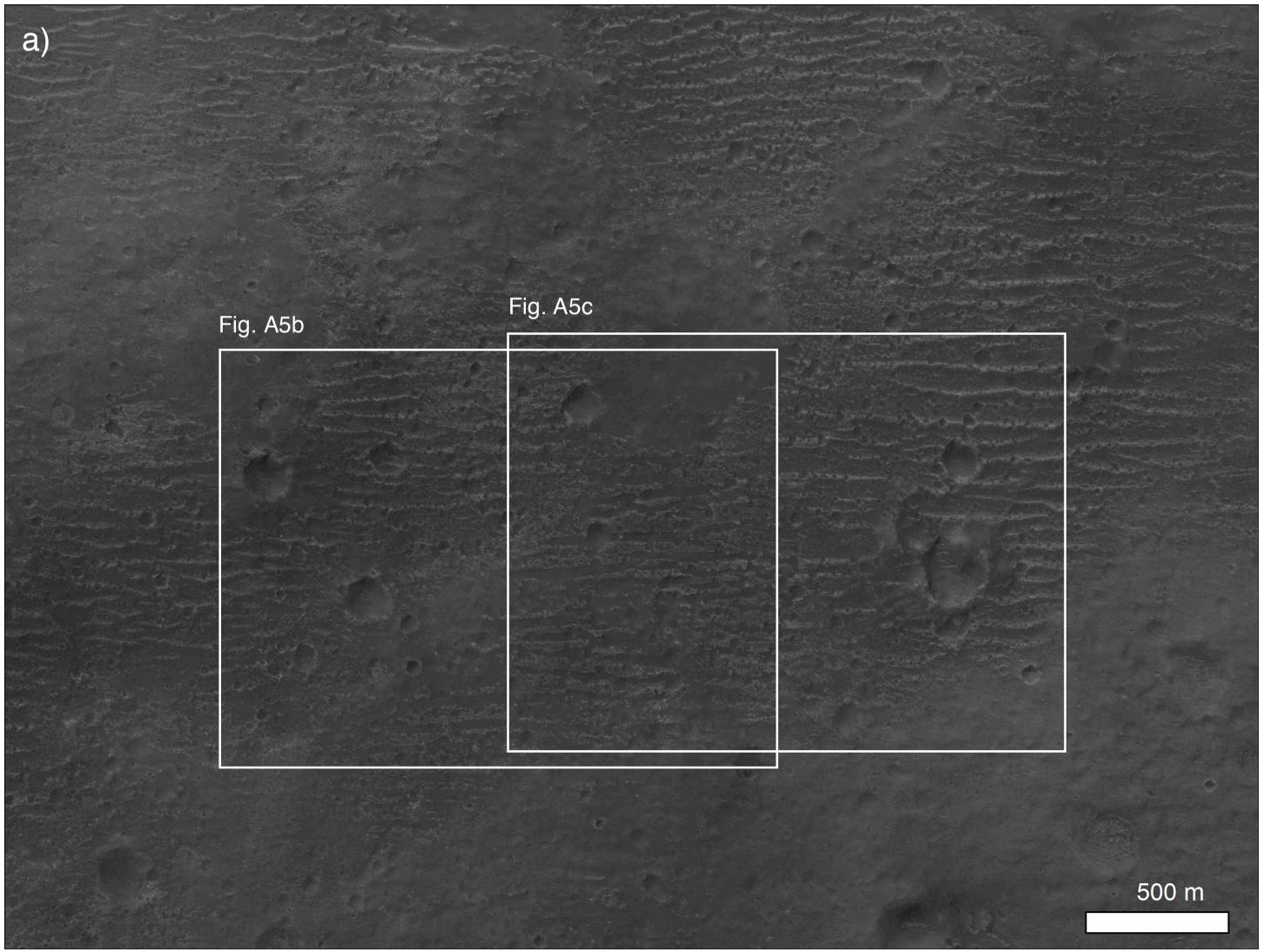

Figure A5. Examples of transition between preserved bedform topography and erosional/remnant 'washboard' morphology. This region is located in the lower right portion of Figure A4b. (a) HiRISE image showing overview of preserved bedforms along the left and right sides and 'washboard' texture in the center due to their partial erosion. Note that the bedforms and 'washboard' morphologies are overlain by a smoother, darker unit that has been largely stripped away in this location.

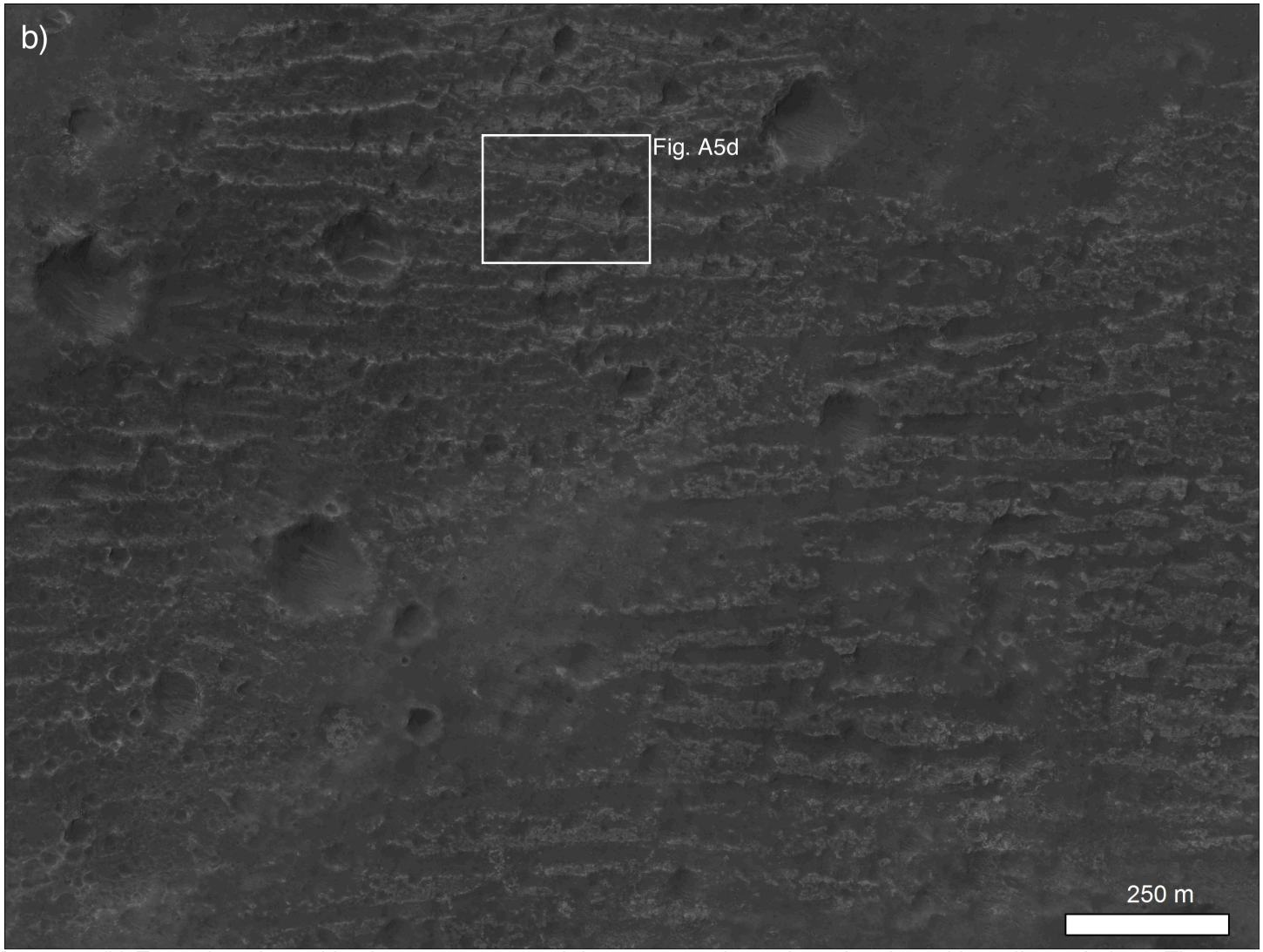

Figure A5, cont. (b) Examples of transition between preserved dune topography and erosional 'washboard' morphology. The (cratered) preserved bedforms are visible in the left half of the image, and the 'washboard' morphology is prevalent in the right. The occurrence of the latter coincides with erosion of the dune crests, suggesting the flat-topped 'mesas' that are characteristic of the washboard morphology may be composed of interdune regions or cemented upper bounding surface of dunes. Such regions may be preferentially cemented due to a rising groundwater table, whereas the dune crests may not be as well-cemented and are thus easier to erode.

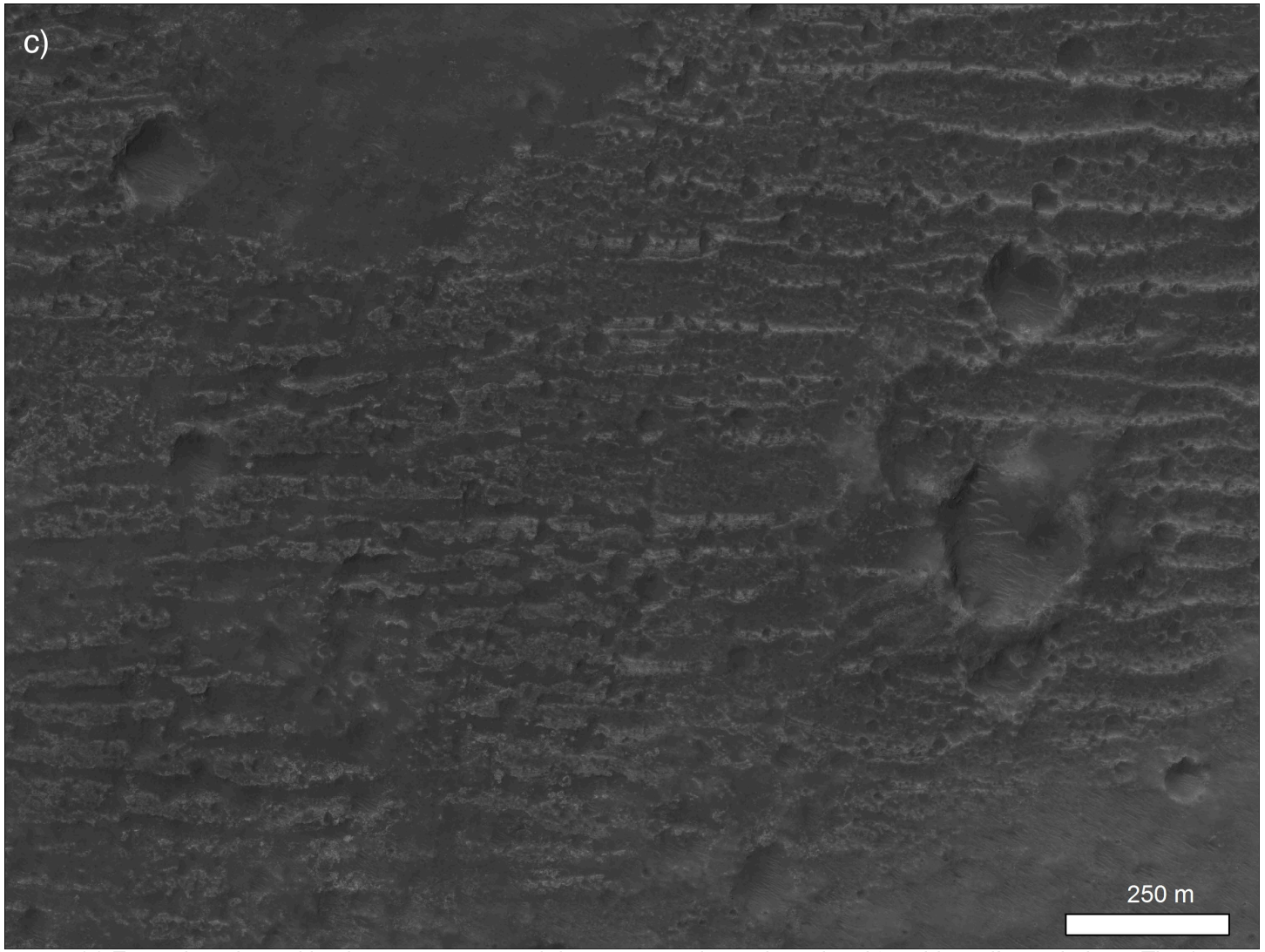

Figure A5, cont. (c) Examples of transition between preserved dune topography and erosional 'washboard' morphology. The (cratered) preserved bedforms are visible in the right half of the image, and the 'washboard' morphology is prevalent in the left. The occurrence of the latter coincides with erosion of the dune crests, suggesting the flat-topped 'mesas' that are characteristic of the washboard morphology may be composed of interdune regions or cemented upper bounding surface of dunes. Such regions may be preferentially cemented due to a rising groundwater table, whereas the dune crests may not be as well-cemented and are thus easier to erode.

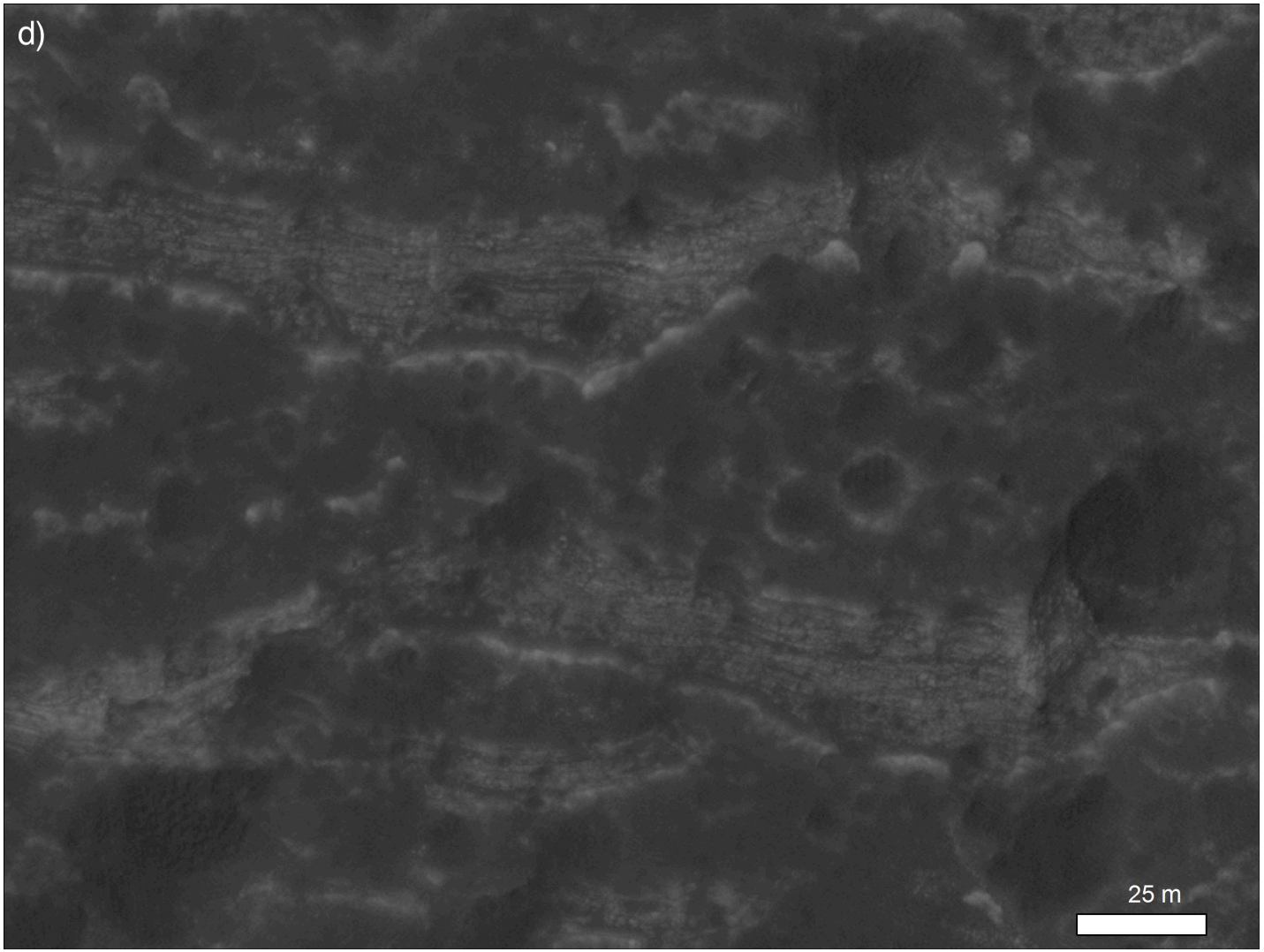

Figure A5, cont. (d) Close-up of transitional region between preserved bedforms and 'washboard' morphology. Here, the dark-toned regions coincide with what appear to be the stoss side and interdune regions of the bedforms and the crests are only partially eroded.The light-toned regions exhibit clear preservation of the internal stratification of the dunes. As the crests are eroded further so are the (apparently overlying) dark-toned materials, creating a more flat-topped mesa morphology that is characteristic of the 'washboards', with light-toned preserved dune regions on either side of the 'mesas'. See Figure A5b for location.

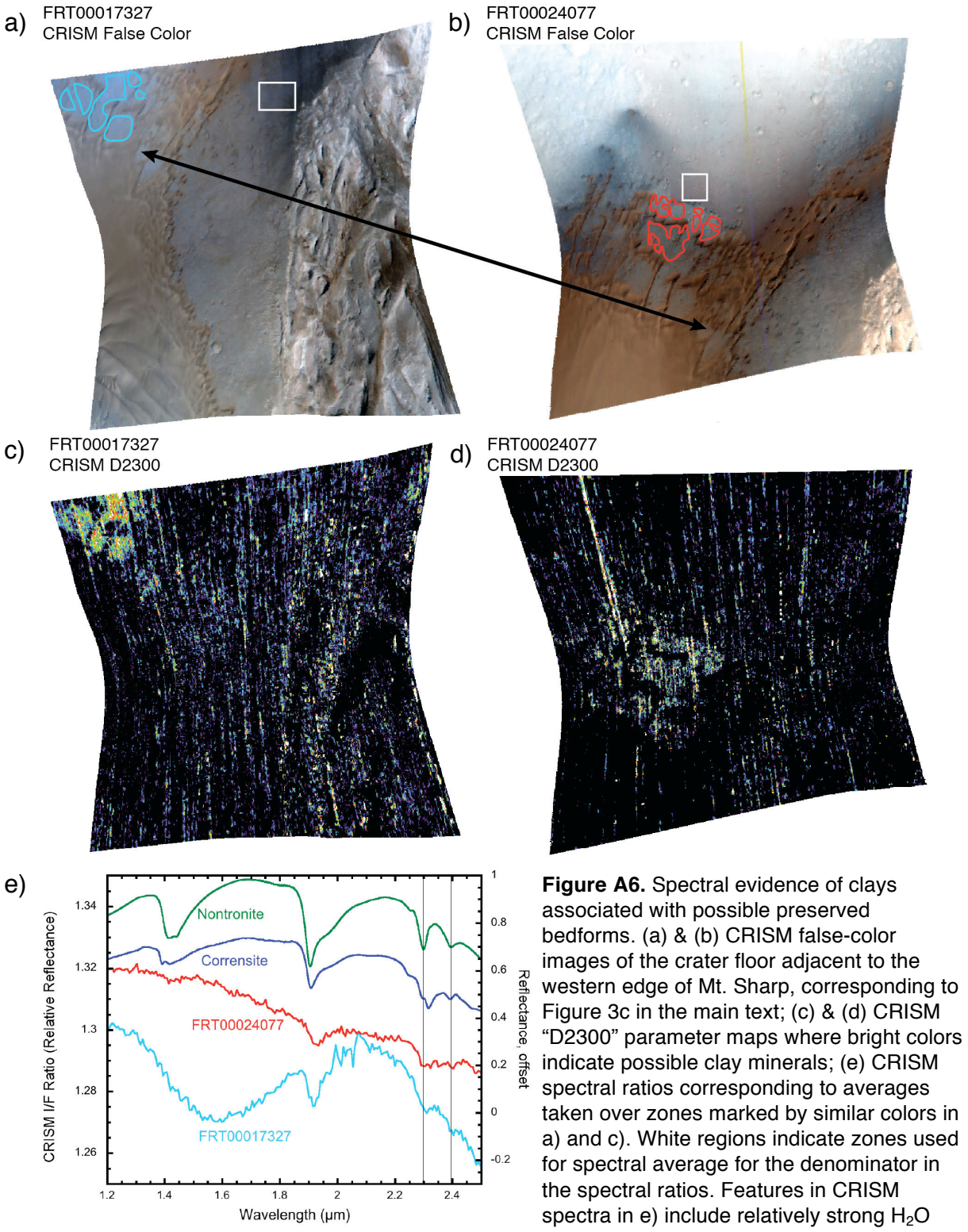

Figure A6. Spectral evidence of clays associated with possible preserved bedforms. (a) & (b) CRISM false-color images of the crater floor adjacent to the western edge of Mt. Sharp, corresponding to Figure 3c in the main text; (c) & (d) CRISM "D2300" parameter maps where bright colors indicate possible clay minerals; (e) CRISM spectral ratios corresponding to averages taken over zones marked by similar colors in a) and c). White regions indicate zones used for spectral average for the denominator in the spectral ratios. Features in CRISM spectra in e) include relatively strong H_2O features at 1.9 μm and weaker Fe/Mg-OH features near 2.3-2.5 μm. These signatures are consistent with smectite or mixed-layer chlorite/smectite, possibly mixed with other hydrous phases.

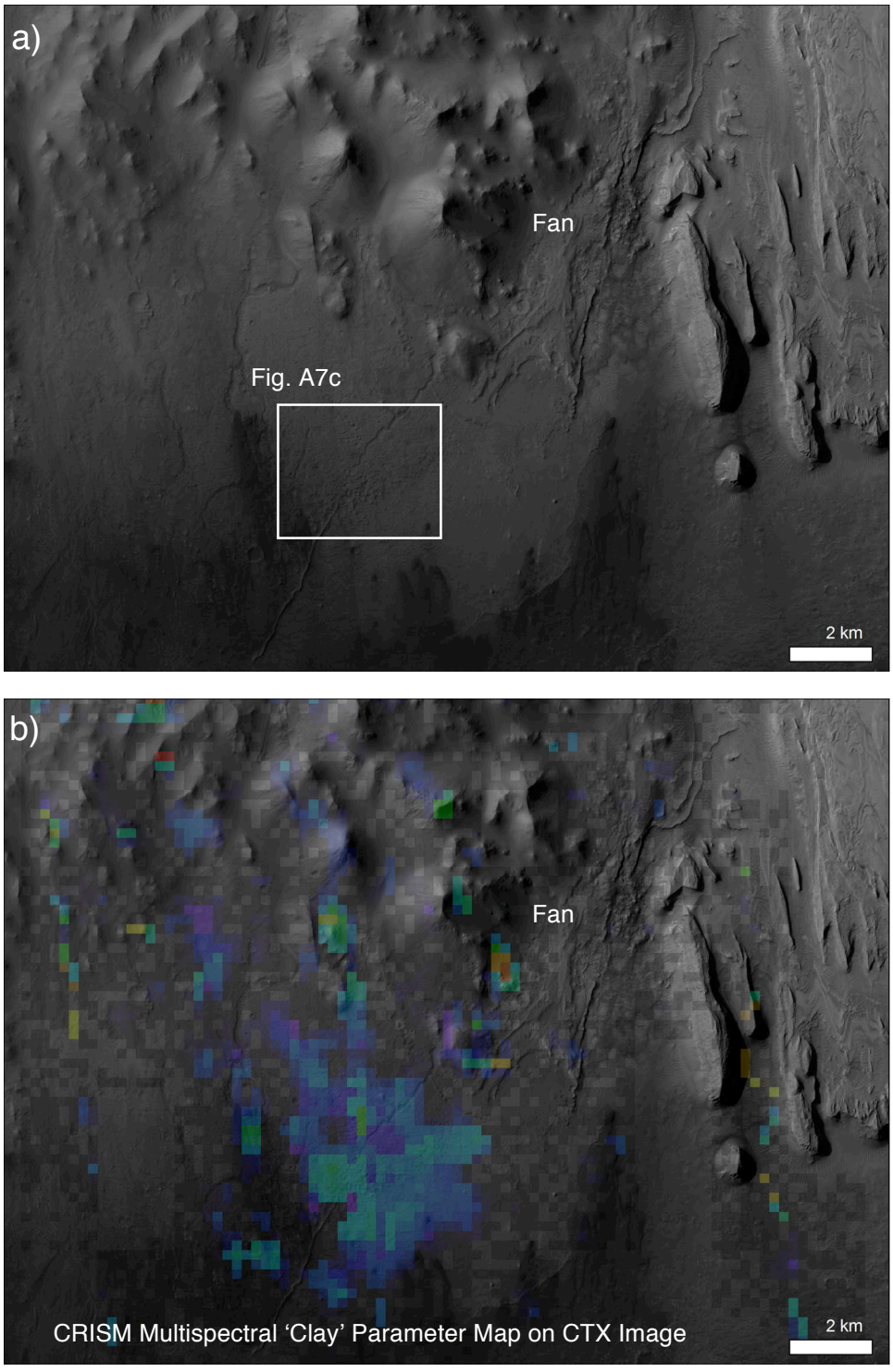

Figure A7. Clay detections associated with preserved bedforms at the distal end of a fan deposit derived from the southern portion of lower Mt. Sharp. (a) Context Camera (CTX) mosaic showing the fan deposit (sourced from Lower fm.) and associated positive/negative relief channel features. (b) CRISM D2300 'clay' parameter map derived from 72 channel, ~200 m/pixel 'mapping' mode data. Bright blue and greenish tones indicate higher potential for clay minerals (drop in reflectance at ~2300 nm).

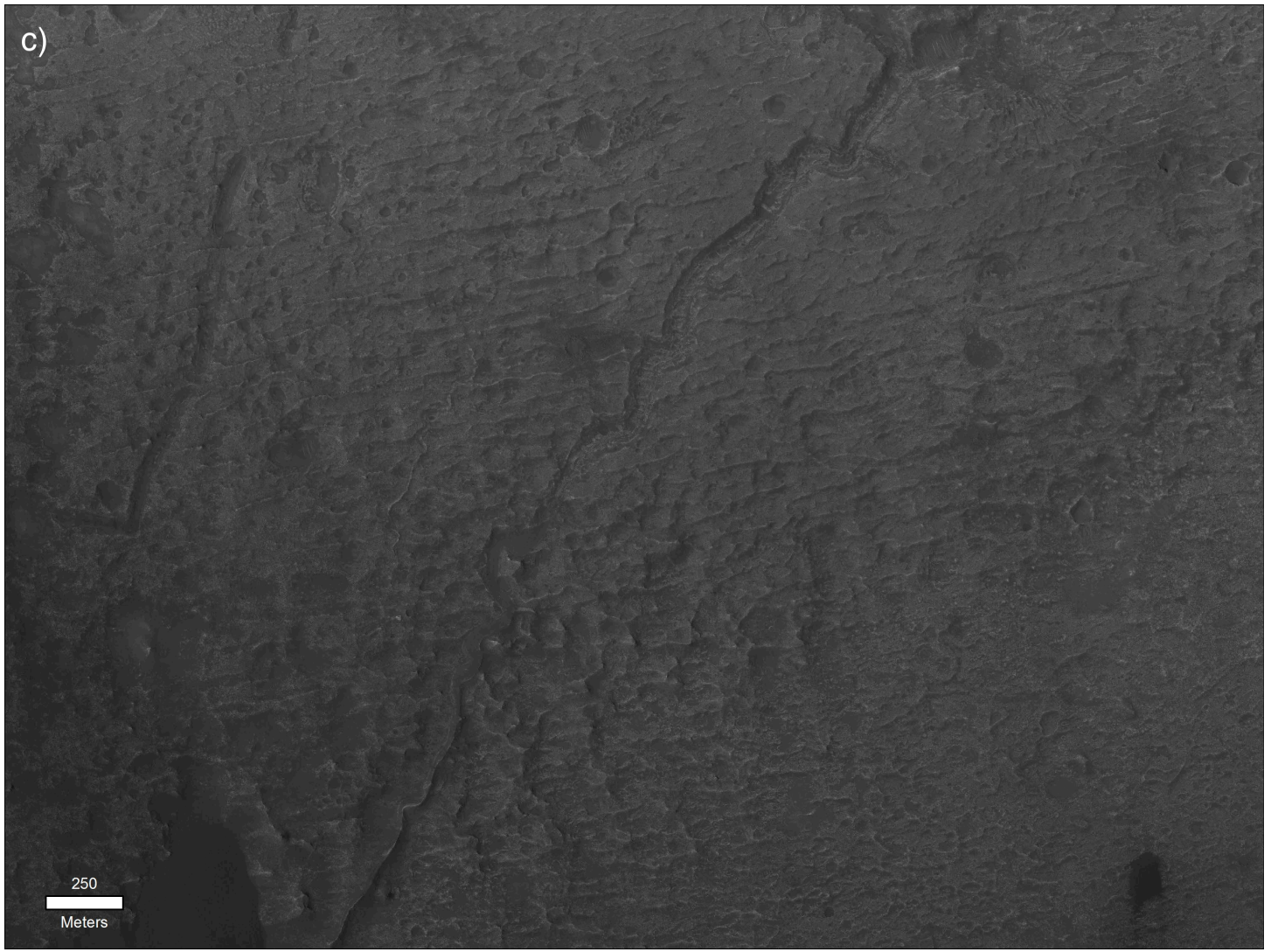

Figure A7, cont. (c) Close-up of CTX image for region exhibiting positive clay detection in CRISM data. Note the sinuous nature and transition from negative to positive relief of the channel feature that runs from the upper right to the lower left. Raised, linear features that trend approximately E-W and that exhibit bifurcation are consistent with preserved bedforms. In this example, the features may represent the original crests and dune topography with apparently minimal erosion. They are revealed as the overlying units, possibly distal sediments associated with the fan, are stripped away.

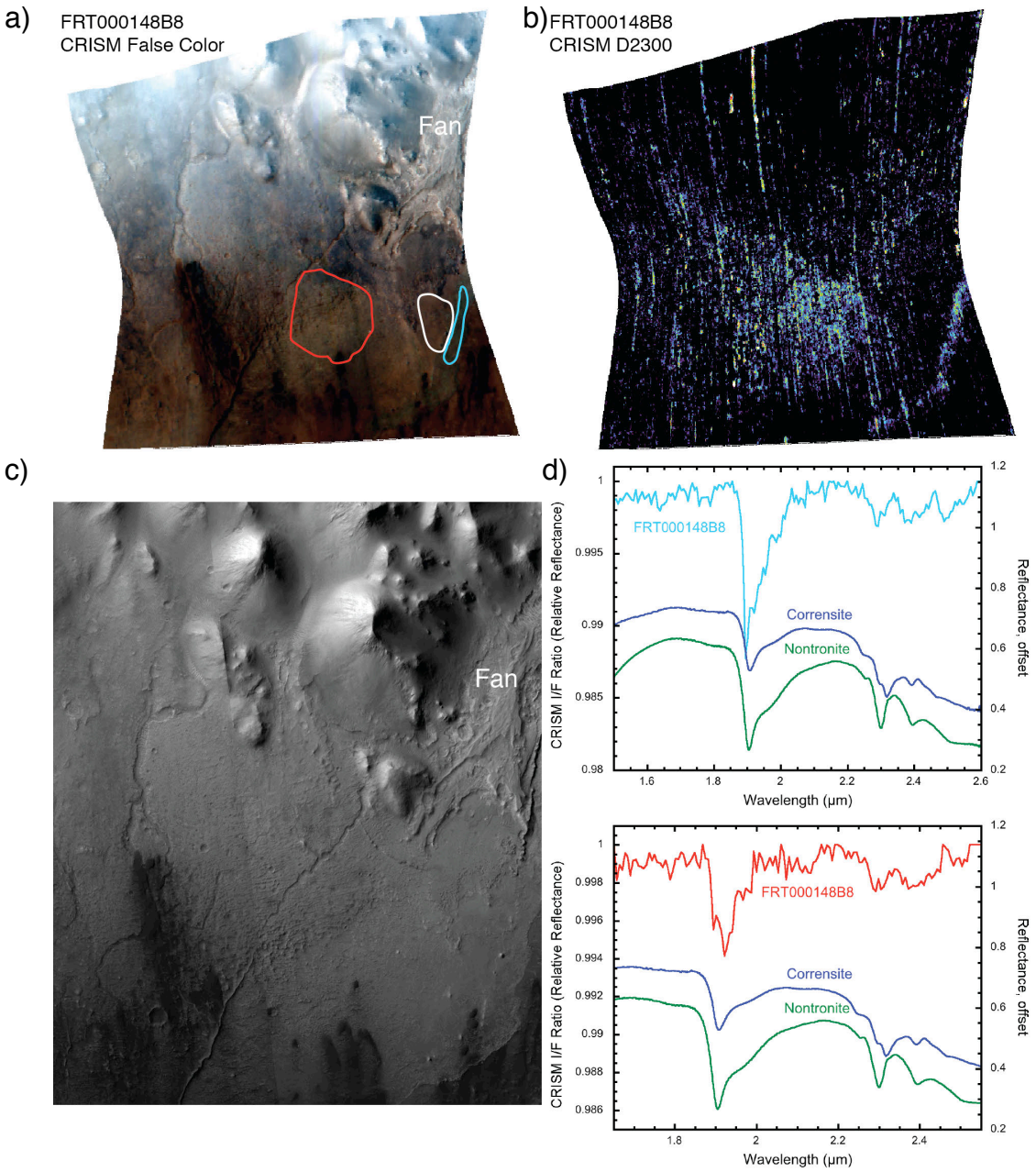

Figure A8. Clay signatures associated with preserved but partially eroded bedforms and a fan deposit along the southern margin of Mt. Sharp. This is the same region as shown in Figure A7. **(a)** CRISM false-color image, ~11 km across; **(b)** CRISM "D2300" parameter map where bright colors indicate possible detections of clay minerals; **(c)** CTX image for region covered in a); **(d)** continuum-removed spectral ratios from zones outlined in similar colors in a). White region in a) indicates ROI used for denominator spectral average. H_2O features near ~1.9 μm in d) are strong relative to metal-OH features at ~2.3-2.5 μm, indicating additional hydrated phases may be present, but the presence of the 2.3-2.5 μm feature even in this relatively noisy high spatial resolution CRISM image confirms the signatures observed in the lower spatial and spectral resolution 'mapping' mode data (i.e., Figure A7b). These absorptions are consistent with Fe/Mg smectite and/or mixed-layer chlorite/smectite. The distinct features at 2.3, 2.4 and 2.5 μm in the cyan spectral ratio are particularly consistent with a smectitic clay.

Table A1. List of HiRISE and CRISM images used in figures for main text.

Figure	HiRISE ID	CRISM ID
1a	N/A	N/A
1b	PSP_006855_1750	N/A
1c	ESP_012551_1750	N/A
1d	ESP_012551_1750	N/A
2a	ESP_025012_1745	N/A
2b	PSP_008147_1750	N/A
2c	ESP_017509_1745	N/A
2d	ESP_017509_1745	N/A
2e	ESP_017509_1745	N/A
3a	ESP_025012_1745	N/A
3b	ESP_025012_1745	N/A
4a	PSP_009294_1750	N/A
4b	N/A	FRT0000C518
4c	ESP_026568_1750	N/A
4d	N/A	FRT00017327

Table A2. List of HiRISE and CTX images used in supporting online figures.

Figure	HiRISE ID	CTX ID
A1b,c	ESP_012551_1750	N/A
A2b	ESP_020555_1750	N/A
A2c	PSP_009595_1755	N/A
A2d	PSP_001488_1750	N/A
A2e	PSP_008147_1750	N/A
A2f	ESP_019065_1745	N/A
A2g	ESP_019065_1745	N/A
A2h	ESP_019065_1745	N/A
A3b	ESP_016586_1755 ESP_013685_1750	N/A
A3c	ESP_013263_1750	N/A
A3d	PSP_009571_1755 ESP_024735_1755	N/A
A3e	PSP_009571_1755	N/A
A3f	PSP_009294_1750	N/A
A3g	ESP_012195_1750	N/A
A3h	PSP_006644_1745	N/A
A3i	PSP_006288_1740	N/A
A4b-h	ESP_025012_1745	N/A
A5	ESP_025012_1745	N/A
A7a,b	N/A	P04_002464_1746_XI_05S221W_070204
A7c	ESP_014397_1745	N/A